

AN INVESTIGATION INTO THE PROMINENCE OF SPIRAL GALAXY BULGES

Alister W. Graham¹

Instituto de Astrofísica de Canarias, La Laguna, E-38200, Tenerife, Spain
 agraham@ll.iac.es

ABSTRACT

From a diameter-limited sample of 86 ‘face-on’ spiral galaxies, the bulge-to-disk size and luminosity ratios, and other quantitative measurements for the prominence of the bulge are derived. The bulge and disk parameters have been estimated using a seeing convolved Sérsic $r^{1/n}$ bulge and a seeing convolved exponential disk which were fitted to the optical (B , R , and I) and near-infrared (K) galaxy light profiles. In general, early-type spiral galaxy bulges have Sérsic values of $n > 1$, and late-type spiral galaxy bulges have values of $n < 1$. Use of the exponential ($n=1$) bulge model is shown to restrict the range of r_e/h and B/D values by more than a factor of 2. Application of the $r^{1/n}$ bulge models results in a larger mean r_e/h ratio for the early-type spiral galaxies than the late-type spiral galaxies. Although, this result is shown not to be statistically significant. The mean B/D luminosity ratio is, however, significantly larger ($> 3\sigma$) for the early-type spirals than the late-type spirals.

Two new parameters are introduced to measure the prominence of the bulge. The first is the difference between the central surface brightness of the galaxy and the surface brightness where the bulge and disk contribute equally. The other test uses the radius where the contribution from the disk and bulge light is equal – normalised for the effect of intrinsically different galaxy sizes. Both of these parameters reveal that the early-type spiral galaxies ‘appear’ to have significantly ($> 2\sigma$ in all passbands) bigger and brighter bulges than late-type spiral galaxies. This apparent contradiction with the r_e/h values can be explained with an iceberg-like scenario, in which the bulges in late-type spiral galaxies are relatively submerged in their disk. This can be achieved by varying the relative bulge/disk stellar density while maintaining the same effective bulge-to-disk size ratio.

The B/D luminosity ratio and the concentration index C_{31} are, in agreement with past studies, positively correlated and decrease as one moves along the spiral Hubble sequence towards later galaxy types. Although for galaxies with large extended bulges, the concentration index no longer traces the B/D luminosity ratio in a one-to-one fashion. A strong (Spearman’s $r_s=0.80$) and highly significant positive correlation exists between the shape, n , of the bulge light profile and the bulge-to-disk luminosity ratio.

The absolute bulge magnitude – $\log n$ diagram is used as a diagnostic tool for comparative studies with dwarf elliptical and ordinary elliptical galaxies. At least in the B -band, these objects occupy distinctly different regions of this parameter space. While the dwarf ellipticals appear to be the faint extension to the brighter elliptical galaxies, the bulges of spiral galaxies are not; for a given luminosity they have a noticeably smaller shape parameter and hence a more dramatically declining stellar density profile at larger radii.

Subject headings: galaxies: formation — galaxies: fundamental parameters — galaxies: photometry — galaxies: spiral — galaxies: structure — galaxies: dwarf

1. Introduction

Hubble (1926, 1936) used three criteria to classify spiral galaxies in what has become known as the Hubble sequence. Based on the structural forms of photographic images, his first criteria was the “relative size of the unresolved nuclear region”. The other criteria were the degree of resolution in the arms, and the extent to which the spiral arms are unwound. Going from early-type (Sa) to late-type spirals (Sc in Hubble’s classification), Hubble wrote that “*the arms appear to build up at the expense of the nuclear regions and unwind as they grow; in the end, the arms are wide open [highly resolved] and the nuclei inconspicuous*”.²

With the above order of criteria reversed, and basing spiral galaxy classification primarily on the characteristics of the arms, Sandage (1961) notes in the ‘Hubble Atlas of Galaxies’ that Sa type galaxies can exist with both large and small bulges, however, a general correlation still exists between the relative size of the bulge and the criteria of the arms (or morphological type). For a review of the Hubble classification scheme, see van den Bergh (1997). Simien & de Vaucouleurs (1986) were bold enough to try placing this trend of decreasing bulge-to-galaxy luminosity ratio with increasing galaxy type on a quantitative basis – fitting a cubic to the observed relation. In order to do this, they compiled a sample of 98 galaxies (from six different sources) with galaxy type $-3 \leq T \leq 7$ – 64 with type Sa or later. They modelled the bulges with an $r^{1/4}$ law and the disks with an exponential profile. Commenting on the standard deviation of 1.14 mag between multiple observations of the same galaxies³, they wrote that “Clearly, there is room for improvement”. The bulge-to-disk size and luminosity ratios from their paper is presented here in Figure 1.⁴

¹Isaac Newton Group, La Palma, Spain

²Hubble also used an additional classification, which was the presence of a bar, giving rise to a parallel sequence of spiral galaxies that followed the above criteria and led to the second prong in the Hubble tuning-fork diagram.

³The standard deviation of 1.14 mag from Simien & de Vaucouleurs (1986) refers to the measured bulge magnitude minus the total galaxy magnitude between similar galaxies observed by different authors. This is the quantity used in their figure 2 and 3.

⁴The Δm_I data from table 4 of Simien & de Vaucouleurs (1986) has been used to compute the B/D luminosity ratios

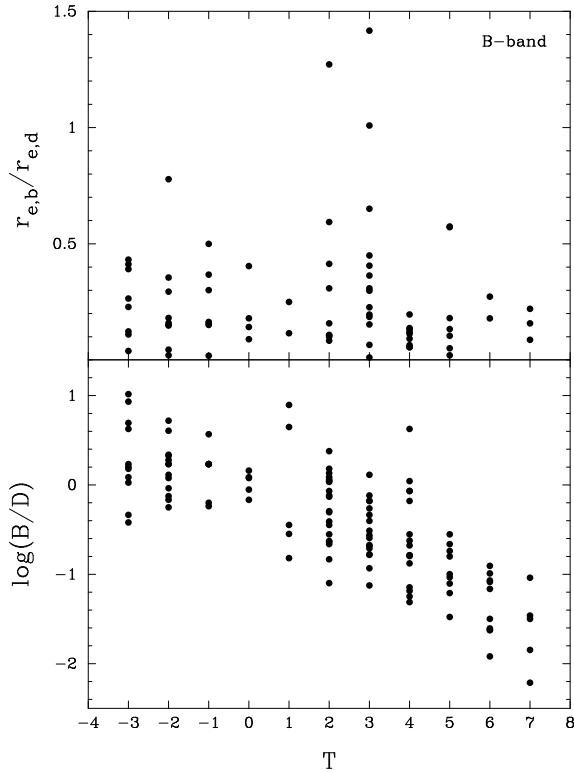


Fig. 1.— This figure shows the bulge-to-disk effective radius ratio $r_{e,b}/r_{e,d}$ (upper panel) and the logarithm of the bulge-to-disk luminosity ratio B/D (lower panel) from the data of Simien & de Vaucouleurs (1986).

More recently, using an exponential (Patterson 1940; Freeman 1970) bulge profile rather than a de Vaucouleurs (1948, 1959) $r^{1/4}$ bulge profile, de Jong (1996b) and Courteau, de Jong, & Broeils (1996) claimed that the bulge-to-disk scale-length (or size) ratio was in fact independent of Hubble type – a result consistent with the data of Simien & de Vaucouleurs (1986). If the bulge-to-disk size ratio is statistically shown to be independent of morphological type, this would imply that the variation in the bulge-to-disk luminosity ratio that characterises the Hubble sequence for spirals is either due to changes in the relative surface brightness of the bulge and disk, and/or changes in the bulge profile shape.

However, before one draws any foregone conclusions, D’Onofrio, Capaccioli, & Caon (1994) have already questioned the applicability of a fitting-function which cannot account for possible variations in the curvature of a bulge’s light profile, and it has since been shown that spiral galaxy bulges are in fact not universally described with either an exponential profile or an $r^{1/4}$ law (Andredakis, Peletier, & Balcells 1995; Moriondo, Giovanardi, & Hunt 1998; Khosroshahi, Wadadekar, & Kembhavi 2000). Rather, a continuous range of bulge light profile shapes are now known to exist. These have been well described by the Sérsic (1968) $r^{1/n}$ profile⁵, and, moreover, it has been shown that early-type spiral galaxy bulges have larger shape parameters n than late-type spiral galaxy bulges.

In fact, in the profile fitting performed by de Jong (1996a), he found that 40% of the spiral galaxy bulges were better modelled with an $n=2$ or $n=4$ model than an exponential model. He statistically showed that, on average, the Sa and Sb galaxies are better modelled with an $r^{1/2}$ bulge light profile than an exponential profile and that the Sbc-Scd galaxies are fit equally as well with the $n=2$ bulge model as the $n=1$ bulge model (see Figure 4 of de Jong 1996a). Furthermore, from the 30 early-type disk galaxies modelled with a Sérsic bulge by Andredakis et al. (1995), only two had shape parameters n consistent with a value 1 or less. Only the late-type (\geq Sd) spiral galaxies in the sample of de Jong were better modelled,

shown here in Figure 1.

⁵The Sérsic model reduces to the $r^{1/4}$ law when $n=4$, and reduces to an exponential profile when $n=1$.

on average, with an $n=1$ profile and possibly even these have true bulge profile shapes significantly different from a pure exponential. Therefore, any investigation into the global bulge-to-disk properties of spiral galaxies that ignores this structural trend will be biased to some degree. Moriondo, Giovanardi, & Hunt (1998) also drew attention to this with a sample of 14 galaxies, revealing how forcing an exponential bulge profile can restrict the full range of galaxy parameters which exist.

Using the model parameters from the ‘best-fitting’ $r^{1/4}$, $r^{1/2}$, or exponential profile from each galaxy in de Jong’s sample, (as determined using the χ^2 values from de Jong 1996a), Graham & Prieto (1999a,b) reinvestigated the claim for a scale-free Hubble sequence. Using the K -band data set of de Jong (1996a), Graham & Prieto (1999a) showed that the average bulge-to-disk scale-length ratio obtained using the exponential bulge model is actually *smaller* (at the 98% confidence level) for the early-type spiral galaxies than the late-type spiral galaxies. In fact, for all passbands used, use of the exponential bulge profile resulted in an average r_e/h ratio that was significantly ($\sim 2-3\sigma$) smaller for the early-type spiral galaxies than that obtained when using the best-fitting profile models. Consequently, failing to account for the different structural profiles, which are dependent on morphological type, seriously affects ones ability to draw any subsequent conclusions about trends between structural properties and galaxy type.

This paper presents a further, more detailed, analysis into the claim that the bulge-to-disk size ratio is independent of morphological type, and goes on to explore the bulge-to-disk luminosity ratio. Rather than simply using the $n=1$, 2, or 4 bulge models, the optical (B , R , I) and near-infrared (K) light profiles from de Jong (1996a) are re-modelled using a seeing convolved Sérsic $r^{1/n}$ bulge and a seeing convolved exponential disk – as described in Section 2. The galaxy sample and best-fitting model parameters are presented in Section 3. Section 4 explores both the bulge-to-disk size and luminosity ratio as a function of morphological type. A preliminary analysis was briefly reported in Graham & Prieto (2000a,b). In Section 5 other quantitative parameters of bulge strength, such as the concentration index, and two new parameters which reflect the visual appearance of the bulge are explored. A summary and

conclusions are presented in Section 6.

2. Sérsic light profiles

2.1. The effects of seeing on $r^{1/n}$ light profiles

The Sérsic (1968) $r^{1/n}$ radial intensity profile can be written as

$$I(r) = I_e \exp \left[-b_n \left\{ \left(\frac{r}{r_e} \right)^{1/n} - 1 \right\} \right] \quad (1)$$

where I_e is the intensity at the effective radius, r_e , which encloses 50% of the light. The term b_n is a function of the shape parameter n , such that $\Gamma(2n)=2\gamma(2n, b_n)$, where Γ is the gamma function and γ is the incomplete gamma function. As given by Capaccioli (1989), this can be well approximated by $b_n=1.9992n - 0.3271$ for $1 < n < 10$. This approximation becomes worse for values of $n < 1$ – as can be seen in Figure 2. Given that many of the spiral galaxy bulges in this sample turn out to have values of $n < 1$, the exact expression for b_n has been used instead of the above approximation. To simplify the appearance of the following equations, the subscript n will be dropped from the term b_n .

Corrections for the effects of seeing have been made using the prescription given in Pritchett & Kline (1981). For any intrinsically radially symmetric, intensity distribution $I(r)$, the seeing convolved profile, $I_c(r)$, is such that

$$I_c(r) = \sigma^{-2} e^{-r^2/2\sigma^2} \int_0^\infty I(x) I_0(xr/\sigma^2) e^{-x^2/2\sigma^2} x dx, \quad (2)$$

where σ is the dispersion of the Gaussian PSF ($=\text{FWHM}/2.3548$), and I_0 is the zero-order modified Bessel function of the first kind (e.g. Press et al. 1986). This approach at correcting the bulge (and disk) profile for seeing was adopted by Andredakis et al. (1995) and later de Jong (1996b).⁶ In this paper, the convolution of equation 2 is applied to both Sérsic bulge models with free shape parameters (i.e. not fixed to integer values) and also to the exponential disk profiles. These convolved models are then simultaneously fit to the light profile data using a standard non-linear least-squares algorithm, which is iterated until conver-

⁶n.b. de Jong (1996b) omitted the negative sign from the final exponent.

gence on the optimal solution giving the smallest χ^2 value.

Figure 3 shows the effects of seeing on various Sérsic profiles with different shape parameters. What is important is the ratio between the dispersion (or FWHM) of the PSF and the effective half-light radii (r_e) of the Sérsic model. Figure 3 has been designed to highlight the most dramatic cases of how seeing can affect the Sérsic luminosity profile. When n is small (e.g. 0.5) and there is a small r_e/FWHM ratio, the original light profile is somewhat akin to a point source and the seeing convolved light profile therefore looks like the PSF. Similarly, when r_e/FWHM is small (e.g. < 2) and the intrinsic light profile falls away quickly with radius, away from the center the seeing convolved profile can be substantially brighter than original profile as the ‘blurred’ light from the brighter inner radii dominates at larger radii. While this may look quite severe in some cases, this effect would be substantially more dramatic if a Moffat (1969) function with say $\beta=2.5$, or any other PSF which has higher wings than a Gaussian (e.g. Saglia et al. 1993, their Figure 1) was used. For the galaxy sample used, all of the derived bulge values for r_e are greater than $1''$, and the ratio r_e/FWHM is greater than 1 for all but three galaxies, and for these galaxies the ratio is only just less than 1.

2.2. The Sérsic bulge to exponential disk luminosity ratio

The ratio of the bulge-to-disk luminosity (B/D) is an important quantity for studies into spiral galaxies. The trend of decreasing B/D luminosity ratio from early- to late-type spirals has since been quantified by, amongst others, Kent (1985) and Simien & de Vaucouleurs (1986) and is regarded as one of the prime characteristic of the Hubble sequence for spiral galaxies.

The total luminosity described by a Sérsic $r^{1/n}$ light profile is given in Graham et al. (1996) as

$$L_{\text{tot}} = \int_0^\infty I(r) 2\pi r dr = \frac{n 2\pi r_e^2 I_e e^b}{b^{2n}} \Gamma(2n), \quad (3)$$

where r_e is in arcseconds. When $n=4$, one obtains the familiar de Vaucouleurs expression $L_{\text{tot}}=7.215\pi I_e r_e^2$ and when $n=1$ one obtains $L_{\text{tot}}=3.803\pi I_e r_e^2$. The total apparent magnitude m_{tot} is simply $-2.5 \log L_{\text{tot}}$, and the total absolute

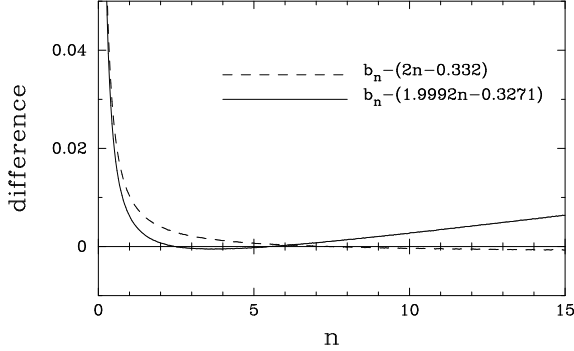


Fig. 2.— This figure shows the difference between the exact value for b_n from the Sérsic $r^{1/n}$ model (equation 1), such that $\Gamma(2n)=2\gamma(2n, b_n)$, and popular approximations used for elliptical galaxies where $n\sim 4$.

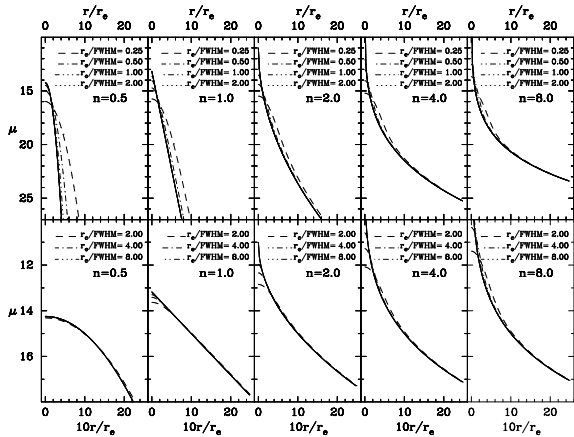


Fig. 3.— The effects of seeing on the Sérsic $r^{1/n}$ profile. The solid lines show a series of $r^{1/n}$ models with $n=0.5, 1.0, 2.0, 4.0$, and 8.0 . The broken lines show the convolution of each model with a Gaussian PSF having a range of ratios between the effective half-light radius of the $r^{1/n}$ model and the FWHM of the Gaussian PSF. The lower panel shows an enlarged view of the inner two effective radii when the effects of seeing are more subtle.

magnitude M_{tot} given by $M=m-5\log(D)-25$, where D is the distance to the galaxy in Mpc.

However, for the disk, rather than use r_e and I_e , it is common practice to use the disk scale-length ($h=r_e/b^n$) and the central surface brightness $I_0=I_e e^b$. From here on, the use of r_e and I_e will refer only to that of the bulge. The ratio of bulge-to-disk luminosities is then given by the expression

$$\frac{B}{D} = \frac{n_b \Gamma(2n_b) e^b / b^{2n_b}}{n_d \Gamma(2n_d)} \left(\frac{r_e^2}{h^2} \right) \left(\frac{I_e}{I_0} \right), \quad (4)$$

where the subscripts b and d on the shape parameter n refer to the bulge and disk respectively, and the parameter b ($=b_n$) refers to that of the bulge. Given that disks are well described by an exponential profile, one can substitute n_d with the value of 1. For integer values of x , $\Gamma(x)=(x-1)!$ and equation 4 can be further reduced to give

$$\frac{B}{D} = \frac{(2n_b)! e^b}{2 b^{2n_b}} \left(\frac{r_e^2}{h^2} \right) \left(\frac{I_e}{I_0} \right), \quad (5)$$

where n_b refers to the shape parameter of the bulge. When $n_b=4$, the factor in the front reduces to 1/0.28 as given in Binney & Merrifield (1998).

It is interesting to note that if the Hubble sequence for spiral galaxies is shown to be scale-free (i.e. independent of the r_e/h ratio), then any variations in the B/D luminosity ratio must be due to changes in the relative surface brightness of the bulge and disk, and/or the shapes of the light profiles of these components.

For the sake of curiosity, to investigate how the first term in equation 4 varies with n_b , Figure 4 shows the relationship between $(n_b \Gamma(2n_b) e^b / b^{2n_b}) / n_d \Gamma(2n_d)$ and n_b , with $n_d=1$.

3. The Data

3.1. The Galaxy Sample

The one-dimensional light profile data⁷ from the statistically complete diameter-limited sample of 86 undisturbed low-inclination (face-on) spiral galaxies presented in de Jong & van der Kruit (1994) is reanalyzed here. A detailed discussion

⁷The data can be found at <http://cdsweb.u-strasbg.fr/htbin/Cat?J/A+AS/118/557>.

of the selection criteria, observations, and data reduction can be found in their paper. In this study, the optical passbands B , R , and I , and the near-infrared K -band data are used. The emphasis will be placed on the near-infrared data set because it is the best tracer of a spiral galaxy's global luminous structure – avoiding the obscuring effects of dust and biasing from a few percent (by mass) of hot young stars. The B -band is presented for comparison with both the K -band data presented here and previous studies of this nature.

Of the 86 galaxies, there is no K -band data for three (UGC 02125, UGC 02595, UGC 12808) and a further five galaxies (UGC 10437, UGC 11708, UGC 12732, UGC 12754, UGC 12845) were imaged under non-photometric conditions. However, for a number of tests performed here it does not matter if the data is photometrically calibrated or not as scale-lengths and bulge-to-disk surface brightness differences are used. In tests where this is important, these five galaxies have been excluded. Three galaxies could not be reliably modelled: UGC 08279 and UGC 12732 had no discernable bulge, and the disk of UGC 6028 has two distinct slopes. UGC 09024 was also excluded because NED gives it's morphological type only as 'S?', and the Sa galaxy UGC 00089 has been excluded as it's bulge parameters are heavily biased by the presence of a strong bar. At this stage all the remaining galaxies are included. Later on, the effect of collectively removing all galaxies with a prominent bar is explored. Therefore, either 78 or 74 galaxies were used in the following K -band analysis – depending on whether or not photometric data was required. In the B -band, this rejection process also left either 78 or 74 galaxies.

The morphological types listed by de Jong (1996a) agree well with the year 2000 database in NED. For only three galaxies is there a difference. de Jong lists UGC 10437 as $T=5$, NED as $T=7$; UGC 10445 as $T=5$, NED as $T=6$; and UGC 09024 as $T=8$, and NED as S? The most up-to-date values have been taken, and UGC 09024 excluded from the final analysis as it's exact Hubble type is not specified in NED.

3.2. Surface brightness corrections

The r_e/h ratio is of course independent of the photometric zero-point. However, the need for photometric corrections are required in this in-

vestigation as the K_{22} radius (the radius where the K -band surface brightness equals 22.0 mag arcsec^{-2}) is used in an attempt to normalise the size of each galaxy. Also, in the K -band, galaxy disks are transparent and their surface brightness depends on the inclination of the galaxy. Therefore, if one hopes to compare galaxies at different inclinations, one must correct the disk surface brightness to some standard, such as the face-on value.

The standard surface brightness inclination correction is given by the expression $2.5C \log(a/b)$, where a/b is the ratio of the semi-major over semi-minor axis. For a transparent galaxy, the more inclined it is, the greater the line-of-sight through the galaxy and hence the surface brightness will appear brighter than it would if the galaxy was face on. This corrective term is therefore applied to reduce the observed surface brightness. The value of C is equal to 0 for an optically thick disk, and equal to 1 for a transparent disk. For the K -band data from this low-inclination sample of spirals, the value of C is set equal to 1 (Graham 2000). For the B -band $C=0$ has been used. For the R - and I -bands the C values from Tully & Verheijen (1997) are used, which are 0.52 and 0.61 respectively.

Corrections for Galactic extinction were made using the extinction data, presented in NED, from the composite IRAS and COBE/DIRBE dust extinction maps of Schlegel, Finkbeiner & Davis (1998). For the sample of spirals used here, these new reddening estimates are noticeably larger than the Burstein-Heiles estimates. The mean reddening value in the B -band is 0.24 mag with the largest correction 1.33 mag (c.f. an average value of 0.14 mag with the Burstein-Heiles data). As Schlegel et al. (1998) used an $R_V=3.1$ extinction curve, $A_K=0.085A_B$ which translates into an average reddening correction of only 0.02 mag in the K -band with the maximum K -band correction 0.11 mag.

Two small additional corrections which de Jong (1996b) did not apply are applied here. The first is the $(1+z)^4$ cosmological redshift dimming. The galaxy sample extends to distances of 8000 km s^{-1} , where the cosmological surface brightness dimming, given by $10\log(1+z)$, is not insignificant at 0.114 mag. The distances tabulated by de Jong (with $H_0=100 \text{ km s}^{-1} \text{ Mpc}^{-1}$ and allowing

for Virgo infall) were converted into redshifts that were used to calculate this correction.

The second correction is the k-correction. Due to the stretching of wavelength with redshift, fixed passbands at the telescope sample different intrinsic wavelengths from galaxies at different redshifts. Heliocentric velocities were used to correct for this – the difference between the redshift observed at the telescope and the Sun is, of course, not significant for this correction. The tables in Poggianti (1997) were used for this correction. No correction for evolution was applied.

A Hubble constant of $H_0=75$ km s $^{-1}$ Mpc $^{-1}$ has been used in the final conversion from arcsec to kpc, and from apparent magnitude to absolute magnitude.

3.3. The best-fitting model parameters

One of the early methods for parametrizing the disk involved ‘marking the disk’, by eye, over the radial range where it’s profile appeared to be linear. Not surprisingly, by construction, this approach gave results that ‘appeared’ to be correct; and in itself there is nothing wrong with this. However, at a basic level, because spiral galaxy light profiles are the superposition of both a disk and a bulge component⁸, the inner part of disk, which may appear to be linear with the outer disk profile, can be biased by the presence of light from the outer parts of the bulge. Such problems with the ‘marking the disk’ method are well known (Giovanelli et al. 1994) and so both components should be fit simultaneously (Kormendy 1977) as was done by de Jong (1996a). One must then decide what structural form to use for the bulge. The estimated central surface brightness of the disk, obtained when simultaneously fitting the disk with first an $r^{1/4}$ bulge and then an exponential bulge can vary by half a magnitude and sometimes much more (Graham 2000). The differences to the bulge parameters are even more dramatic, and so exactly which bulge profile shape one uses is an important consideration.

Although de Jong (1996a) noted that a range

⁸At a more refined level, spiral galaxy light profiles are the superposition of several components, such as, in addition to the dominant bulge and disk components: lenses, rings, and bars, which, from a careful 2D image analysis, can also be modelled for some galaxies (Prieto et al. 1997, 2000).

of bulge profile shapes do exist, and that this together with the sky background uncertainty are the two most important sources of error, he presented reasons for having not modelled these structural differences. Firstly, for most of the galaxies, his code for fitting an $r^{1/n}$ bulge model converged on physically unacceptable negative values for the model parameters. This problem was solved here by the inclusion of boundaries to the parameter space which was searched – as done by Schombert & Bothun (1987) who recognised the need for physical limits to what is a purely numerical method. Secondly, de Jong commented that for many of the late-type spiral galaxies the bulge light dominates over the disk light for only a few data points which makes it hard to accurately limit the shape of the bulge. This is true for galaxies with small bulges and so error estimates are useful to gauge this problem. However, it is noted that in fitting the bulge and disk simultaneously, the fitting of the bulge is not solely restricted to those few inner points, but is additionally constrained by data points further out – even though the disk dominates in this region.

For each galaxy, the best-fitting seeing-convolved Sérsic bulge model and exponential disk model were derived three times. The difference was that in the second and third derivation, the uncertainty in the sky-background level was respectively added and subtracted from the light profile data. This was also the approach used by de Jong (1996a) to estimate the errors on the model parameters. For a handful of galaxies, subtraction of the sky-background error resulted in a negative intensity for some of the outer data points in the light profile. When this happened, these points were removed and the fitting proceeded as normal. Similarly, the error on the B/D luminosity ratio represents the B/D luminosity ratio obtained when the uncertainty to the sky-background level was added and subtracted from the light profile.

One source of error which is not dealt with explicitly in this analysis of the 1D light profiles is the presence of third components – such as a bar. For 23 of the 86 galaxies modelled by de Jong, the introduction of bar improved his 2D fits at some level. The statistical analysis which follows is however performed including and excluding these galaxies. Sometimes this had an effect, and other times the reduced number statistics simply weak-

ened the significance of a result. Another issue pertaining to the model parameters is that of coupling. In the fitting process, when a model parameter deviates from its optimal value the other parameters try to adjust themselves so as to keep the χ^2 value as small as possible. This situation not only exists when fitting an $r^{1/n}$ bulge model, but also when fitting an $r^{1/4}$ or an exponential bulge model. One way to gauge the extent of such ‘coupling’ could be to vary one parameter, while allowing the other parameters to compensate, until the χ^2 value increases by some fixed amount. This was the approach taken in Graham et al. (1996), where it was shown that coupling of the $r^{1/n}$ model parameters in fits to brightest cluster galaxies (ellipticals) is not responsible for the trend between profile shape n and galaxy size r_e . However, as was noted before, for spirals with relatively small bulges, the global χ^2 statistic can be rather insensitive to changes in the bulge model and so it is not an appropriate quantity to use here. One could try using the χ^2 value within $2r_{b-d}$, but to do this one would have to fit the bulge and disk models to this radial range alone. In so doing one would no longer be measuring the best global solution which is what one wants. It’s a little like fitting a model nose and body to the silhouette of an elephant. The goodness of the fit is dominated by the model for the body irrespective of whether you fit an ear or a nose to what should be the nose. That is, one may fit significantly different shapes for the nose, while the global χ^2 value changes little. In an attempt to better gauge the goodness of the fit to the nose, one could zoom in, changing all the model parameters, and try to increase the quality of the fit in just the area around the nose – but this would come at the expense of a good fit for the body. One can, and should, fit both the nose (bulge) and body (disk) simultaneously to find the best fit (Schombert & Bothun 1987). Although, when one does this, the goodness-of-fit in the area around the nose certainly does not have to be the best fit for that specific area, and different model parameters may well give a better fit in that region, albeit, at the expense of the global fit. Despite all this, when the shape parameter n was changed from the optimal solution to the traditional values of 1 and 4, Figure 6 reveals that any possible coupling between the model parameters was not sufficiently large as to prevent significant

increases to the χ^2 values over those obtained with an $r^{1/n}$ bulge and an exponential disk model.

The global fits are shown in Figure 21, where the models are represented by the dashed lines, and the seeing-convolved models are represented by the solid lines, which, in most instances, predominantly over-lap each other. While an exponential model fits the disks extremely well in most cases, there are a few exceptions besides the galaxy UGC 6028, which, as mentioned before, has been excluded. This can be seen, for example, in the profile residuals of UGC 05842 and UGC 12614. These two galaxies possess disks which appear to have a shape parameter $n < 1$. In fact, about a dozen galaxies possessed disks which deviated from a straight exponential light profile. These departures may be real for the galaxies: UGC 00490, UGC 06453, UGC 07169, UGC 07901, and UGC 00242. While for other galaxies it may simply be due to errors in the estimate of sky background level which cause the outer few data points to depart from an exponential profile.

To avoid such data points which may be wrong due to an incorrect sky-background estimate, suspect points have been marked in Figure 21 with a circle and excluded from the fitting procedure. In some cases, not performing this truncation actually resulted in the bulge model kicking up and contributing more light to the outer portions of the galaxy than the disk. This situation, illustrated in Figure 5 arises because of the failure of the exponential disk model to allow for curvature in the outer profile. The bulge, able to account for such curvature, comes into play by adding light to the disk in the outer parts of the galaxy and reducing the χ^2 value of the fitted models. Such fits could be telling us that the bulges of some spiral galaxies are a lot more extended and prevalent than previously thought; although, this seems unlikely as the spiral structure usually dominates the light from the outer parts of the images. This example also serves to illustrate the point that secondary minima exist within the ocean of χ^2 values arising from all the different model parameter combinations. Depending on the initial estimates which one provides for the model parameters, one may end up in one of a number of unfavorable minimum. However, while this occurred for 10–20% of the sample after the first run through, a visual inspection of the model fits and the pro-

file data easily revealed when the program had converged on an undesirable minimum (as in Figure 5). For those galaxies which were sensitive to poorly matched initial estimates for the model parameters, the code was run again with initial estimates that more closely resembled the galaxy profile. The results are presented in Figure 21. This situation highlights the fact that one cannot always be passive and blindly run their minimization codes faithfully believing that they will always find the optimal physically realistic solution. However, one can increase their chances by using smarter codes which can climb their way out of local minimum to locate the global minimum.

The χ^2 statistic has been used as an estimator for the quality of the fit. However, a variant of what might be considered the usual practice has additionally been employed. For a number of the galaxies, compared to their disk, their bulge appears relatively small and the global χ^2 value is dominated by the fitted exponential disk, largely irrespective of the bulge model. Clearly, in such circumstances, the global χ^2 statistic is largely insensitive to the bulge model. Therefore, to estimate the goodness-of-fit of the bulge and disk model, the χ^2 values within two times the radius where the bulge and disk light contribute equally ($r_{b=d}$, see Section 5.2) were measured. For three galaxies whose bulge light was less than the disk light even at the center of the galaxy, the inner 3'' radius was used. It should be noted that the bulge and disk model have still been fitted to minimize the global χ^2 value, and not the χ^2 value within $2r_{b=d}$. As a consequence, in some instances use of the $r^{1/n}$ bulge and exponential disk model may result in a larger χ^2 value than the classic bulge models over this radius. However, in general this is not the case as is illustrated in Figure 6, which plots the ratio of the χ^2 values from the different models as a function of n . One can see that both globally, and over the inner $2r_{b=d}$, the $r^{1/n}$ bulge model results in a better fit than the fixed $n=1$ or 4 models.

To inspect whether the fits from the use of an $r^{1/n}$ bulge provide, on average, a statistically significant improvement over the fits from the use of the classical bulge models, Student's t-test was applied to the distributions of χ^2 values. The fits with the $r^{1/n}$ bulge models gave significantly (99.5%) smaller χ^2 values – within $2r_{b=d}$ – than

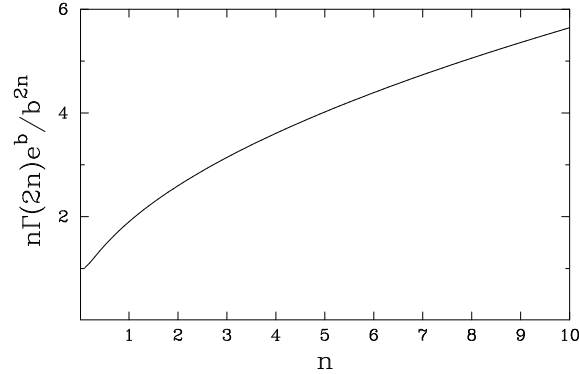


Fig. 4.— This plot reveals the bulge-to-disk luminosity dependence on the bulge shape parameter n , as given in equation 4 (with $n_d=1$).

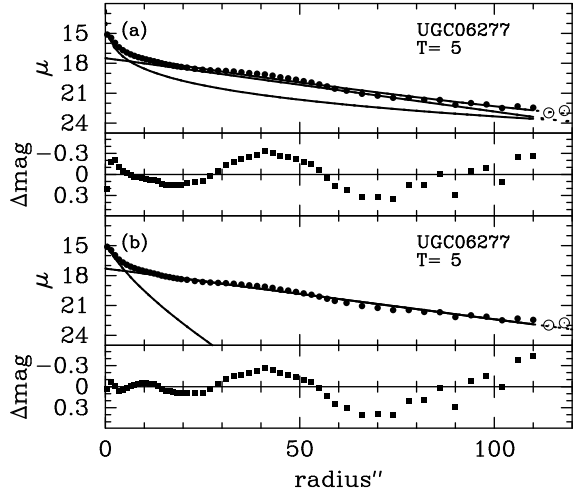


Fig. 5.— This plot illustrates, with the K -band data from UGC 06277, that secondary minima can exist in the ocean of χ^2 values resulting from different light profile model parameters. In the upper panel (a) the χ^2 value is 1.70, and in the lower panel (b) $\chi^2=1.63$. In panel (a), the use of poor initial estimates for the model parameters resulted in the minimization code getting trapped in a local minima and leading to a poor match to the shape of the bulge profile. The dotted curves are the models, while the solid curves are the seeing convolved models which are fitted to the data.

the fits with an exponential bulge model, and smaller still values (at the 99.98% level) than those obtained when using the classical $r^{1/4}$ bulge and exponential disk model.

Figure 7 reveals that not only is there a positive correlation between n and the bulge effective radius (a result also seen in Khosroshahi et al. 2000; their figure 3), but that most of the bulge luminosity profiles are not consistent with an exponential light distribution. In the K -band, only 5 galaxies have a bulge shape parameter n that is consistent with the exponential value of 1. Figure 8 shows the distribution of n with the effective bulge surface brightness.

In Figure 9 a trend can be seen between galaxy type, or numerical stage index T (de Vaucouleurs et al. 1991), and the light-profile shape of a spiral galaxy's bulge. The early-type spiral galaxies have bulges which are better described with shape parameters $n > 1$, while late-type spiral galaxy bulges are better described with shape parameters $n < 1$. This result expands – into the domain of late-type galaxies – upon the trend of decreasing n with increasing T which was observed by Andredakis et al. (1995; their figure 5a) for disk galaxies with morphological type $T \leq 5$. The shape parameter n is therefore more than just an additional parameter that improves the quality of the fitting routines, but traces a physical characteristic of the bulges of disk galaxies. The inner light profiles of late-type spiral galaxy bulges are flatter than those in early-type spiral galaxy bulges and decline more quickly with radius in the outer parts.

A plot of n against the B/D luminosity ratio is shown in Figure 10. In the K -band, the Pearson correlation coefficient between n and $\log(B/D)$ is 0.75, and the Spearman rank-order correlation coefficient is 0.80, with the two-sided significance level of its deviation from zero less than 10^{-18} (that is, this correlation is highly significant). In the B -band these values are 0.60 and 0.70 respectively, with similarly high significance. The current extension to later type spiral galaxies supports and strengthens the correlation between n and the B/D luminosity ratio seen in Andredakis et al. (1995), where they reported a linear correlation coefficient of 0.54 at a significance level of 99.7% for their K -band sample of early-type disk galaxies.

The data were re-modelled using a seeing-

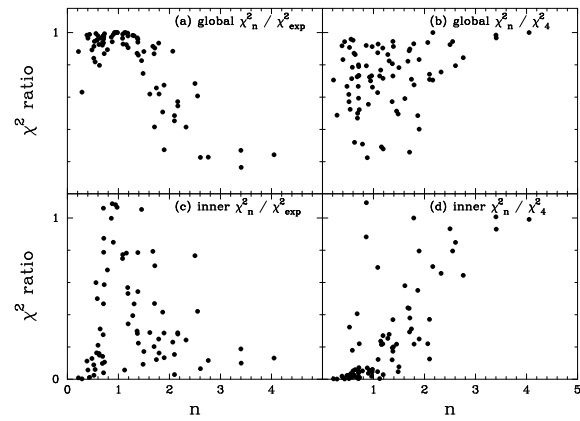


Fig. 6.— The χ^2 values from the $r^{1/n}$, $r^{1/4}$, and exponential bulge models, fitted simultaneously with an exponential disk model to the K -band light profiles, have been given the subscripts n , 4, and exp. The upper panels (a) and (b) show the ‘global’ χ^2 ratios fitted to the entire light profile, while the lower panels (c) and (d) show the χ^2 ratios from the profile within the two times the radius where the bulge and disk light contribute equally. The same best-fitting model parameters, as determined from the global fit, have been used in both the upper and lower panels.

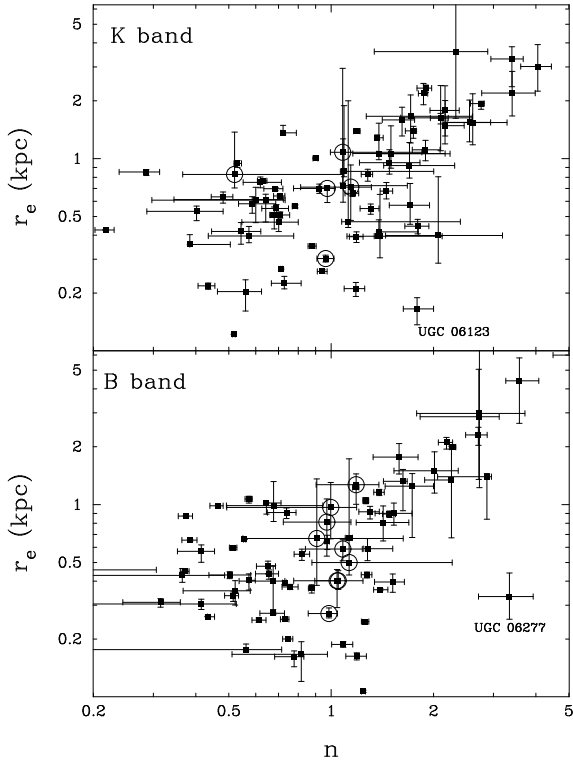


Fig. 7.— The bulge effective half-light radius r_e is plotted against the Sérsic $r^{1/n}$ bulge shape parameter n . The errors are from the uncertainty in the sky-background level. Those data points with circles around them are consistent with a value of $n=1$.

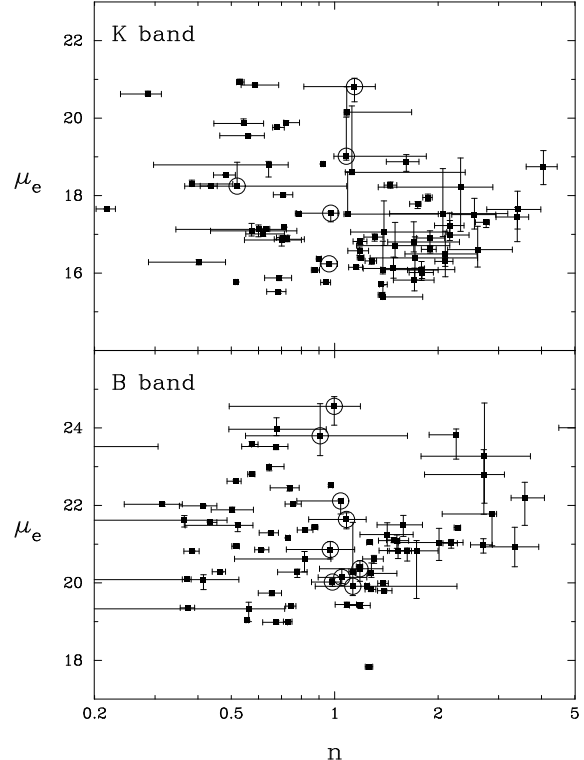


Fig. 8.— The surface brightness, μ_e , of the bulge profile at r_e , is plotted against the Sérsic $r^{1/n}$ bulge shape parameter n . The errors are from the uncertainty in the sky-background level. Those data points with circles around them are consistent with a value of $n=1$.

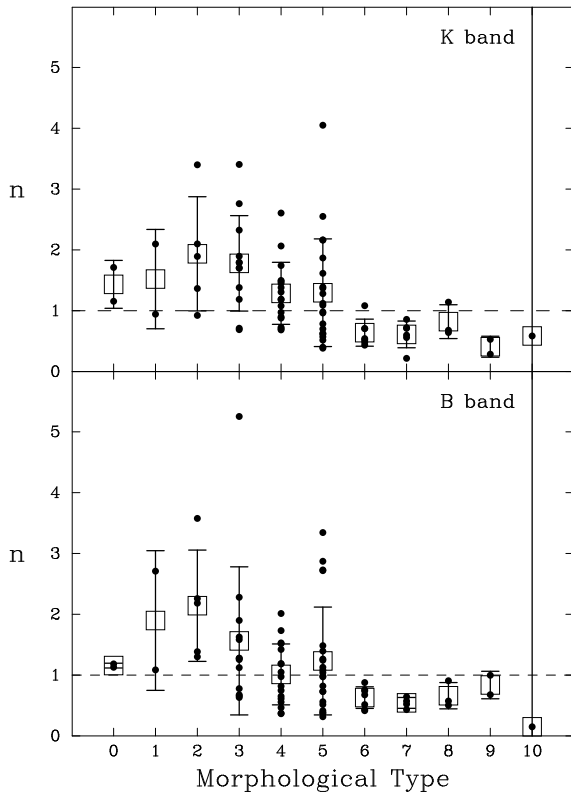


Fig. 9.— For each galaxy, the best-fitting Sérsic $r^{1/n}$ bulge shape parameter n is plotted against the galaxy's morphological type index.

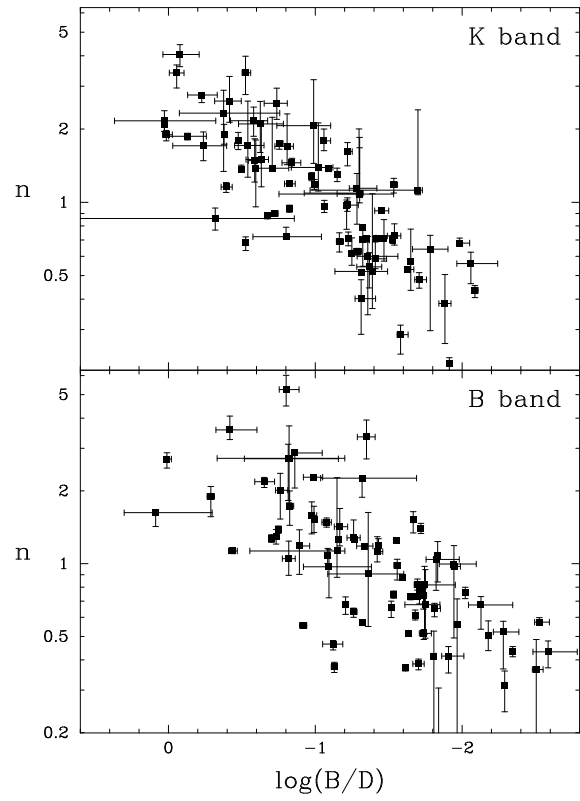


Fig. 10.— For each galaxy, the best-fitting Sérsic $r^{1/n}$ bulge shape parameter n is plotted against the logarithm of the bulge-to-disk luminosity ratio.

convolved exponential bulge model and a seeing-convolved exponential disk model. In Figure 11 the effective bulge radius derived from fitting a Sérsic bulge is plotted against the effective bulge radius derived from fitting an exponential bulge. One can clearly see that fitting an exponential law to the bulge of a spiral which has a Sérsic index greater than 1 will lead to an under-estimation of the true effective bulge radius. On the other hand, if the bulge light profile shape is better described with a Sérsic index less than 1, fitting an exponential bulge will result in over-estimation of the effective bulge radius. Even when just considering galaxies with bulge values of n ranging from 0.5 to 2.0, the range of r_e computed using an exponential bulge is a factor of 2 less than the real range. Changes to the r_e/h ratio are dominated by changes in r_e rather than changes in the disk scale-length h . Differences to the bulge-to-disk luminosity ratio are shown in Figure 12, where it can be seen that use of an exponential bulge model systematically under-estimates the bulge luminosity when the bulge profile shape has $n > 1$, and subsequently results in an under-estimation of the bulge-to-disk luminosity ratio. When n is smaller than 1, the exponential bulge model results in an over-estimation of both the bulge luminosity and the bulge-to-disk luminosity ratio.

Figure 13 shows that the total bulge light (in both the B - and K -band) – and therefore possibly bulge mass – also correlates strongly with the shape of the bulge light profile (Pearson's $r=0.68$, Spearman's $r_s=0.69$). Such behaviour is also seen in the bulge data of Andredakis et al. (1995; their figure 6b). Systematic trends in the shape of the light profile with luminosity have been seen before amongst the dwarf elliptical population (Caldwell & Bothun 1987; Binggeli & Cameron 1991) and parametrized with the Sérsic model (Davies et al. 1988; Young & Currie 1994, 1995; Jerjen & Binggeli 1997; Jerjen, Binggeli, & Freeman 2000). Similarly, this same behaviour of increasing Sérsic shape parameter n with absolute luminosity has been seen amongst the elliptical galaxy population (Michard 1985; Schombert 1986) and subsequently parametrized (Caon, Capaccioli, & D'Onofrio 1993; D'Onofrio, Capaccioli, & Caon 1994; Hjorth & Madsen 1995; Graham & Colless 1997, Gerbal et al. 1997; Lima Neto 1999). Indeed, this pattern has also been observed amongst the

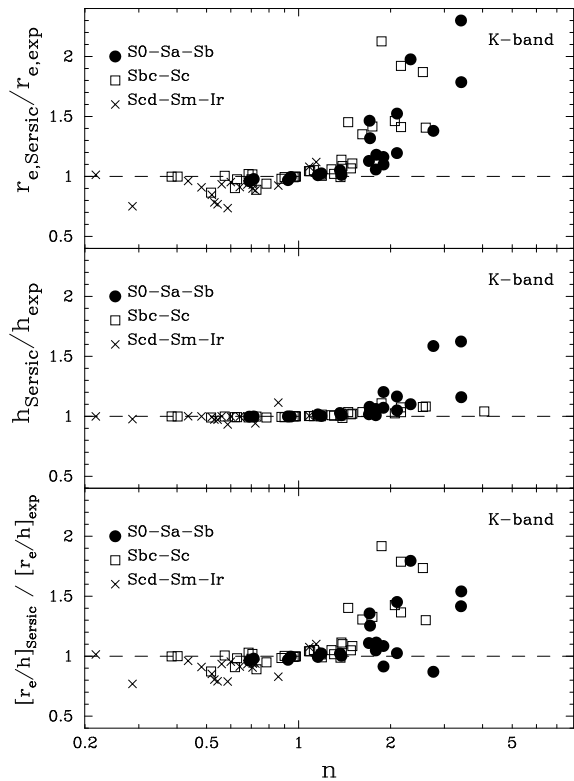


Fig. 11.— A comparison plot of the bulge effective half-light radii r_e , the disk scale-length h , and the ratio of these quantities r_e/h , between the estimates using the best-fitting Sérsic $r^{1/n}$ bulge versus an exponential bulge. An exponential disk was simultaneously fitted in both instances.

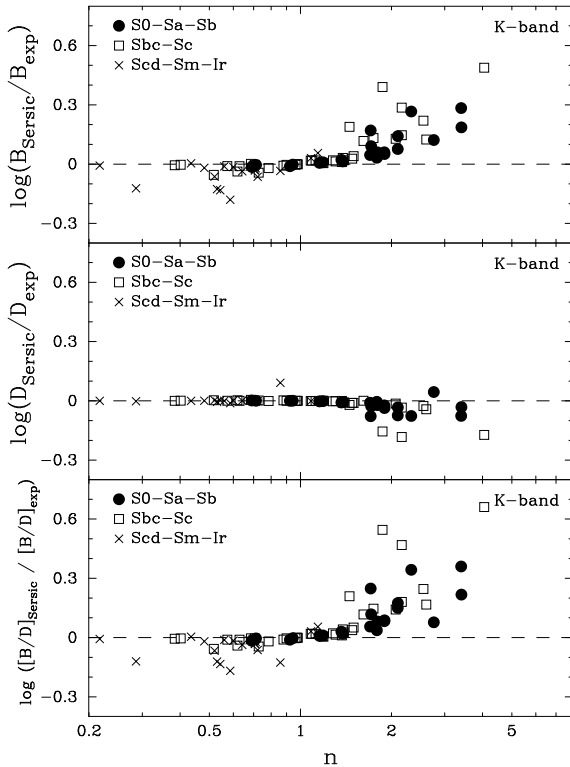


Fig. 12.— A comparison plot of the bulge luminosity B , the disk luminosity D , and the ratio of these quantities B/D , between the estimates using the best-fitting Sérsic $r^{1/n}$ bulge versus an exponential bulge. An exponential disk was simultaneously fitted in both instances.

bulges of S0 galaxies (Capaccioli 1987, 1989). It is therefore of interest to compare all of these objects on the one diagram to look for similarities and differences. The lower panel of Figure 13 is an extension of the plot shown in Jerjen & Binggeli (1997, their figure 2). The dwarf Elliptical (dE) photometry is from the Virgo dEs given in Binggeli & Cameron (1991, 1993) – most recently presented in Jerjen, Binggeli, & Freeman (2000, their figure 6). A Virgo distance-modulus of 31.05 mag has been used (Jerjen, Freeman, & Binggeli 2000). The ‘ordinary’ elliptical galaxy data set are from the Virgo and Fornax Ellipticals presented in Caon et al. (1993) and D’Onofrio et al. (1994), excluding 3 galaxies, from a total of 38, which were labelled as having a ‘poor’ profile fit, and excluding the one E pec galaxy. A Virgo-Fornax distance-modulus of 0.25 mag was used (Graham 1998, and references within).

Viewed on its own, the middle panel of Figure 13 appears to show that the bulges of spiral galaxies form the faint extension to the elliptical galaxies. However, the location of the dwarf ellipticals in the lower panel reveals that this picture is not so clear. Given that, at least structurally, the dwarf elliptical galaxies are the smaller, fainter counterparts to the brighter ellipticals (Caon et al. 1993; Graham et al. 1996; Jerjen & Binggeli 1997), the bulges of spirals show a distinctly different behaviour to the ellipticals. For a given luminosity profile shape, i.e. n , spiral bulges are brighter than ellipticals with the same light profile shape, or alternatively, for a given luminosity, spiral bulges have a shallower core distribution of stars and a steeper fall-off at larger radii (i.e. smaller n). Perhaps the rotating disk is responsible for truncating the bulge and creating the smaller n parameters. However, what is the cause and what is an effect is not clear. What is clear is that the abandonment of the limited classical fitting functions has given rise to a potentially powerful diagnostic tool.

4. Analysis of the bulge-to-disk ratios with morphological type

4.1. Bulge-to-disk size ratio

Graham & Prieto (1999a) showed that the universal application of an exponential light-profile model to the bulges of spiral galaxies produced a mean r_e/h value that was actually smaller for the

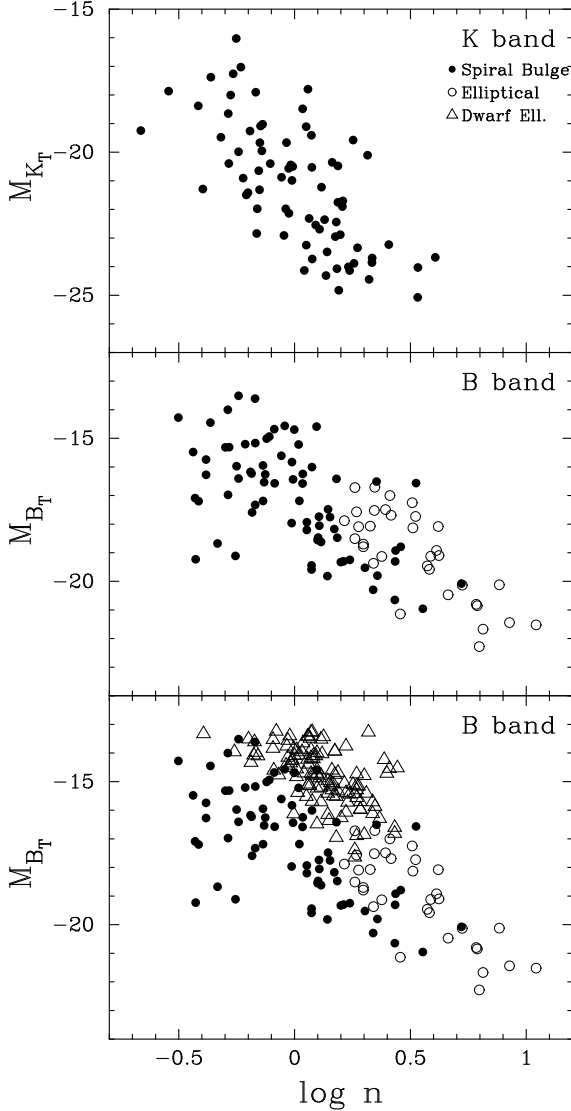


Fig. 13.— The total absolute magnitude of the spiral galaxy bulges is plotted against the logarithm of the best-fitting Sérsic shape parameter. For comparison, a sample of Virgo dwarf elliptical (dE) galaxies from Jerjen, Binggeli, & Freeman (2000) is shown, as are a sample of ‘ordinary’ Virgo and Fornax Elliptical (E) galaxies from Caon et al. (1993) and D’Onofrio et al. (1994). A Hubble constant of $75 \text{ km s}^{-1} \text{ Mpc}^{-1}$, and a Virgo distance-modulus of 31.05 have been used.

early-type galaxies than for the late-type galaxies – at the 98% significance level using the K -band data of de Jong (1996a). This result was clearly at odds with the popular conception of what early- and late-type spiral galaxies look like and brought us to examine the use of the exponential bulge model for drawing conclusions about the nature and structural properties of spiral galaxies.

Fitting an $r^{1/n}$ bulge – which allows for the range of structural profile shapes that spiral bulges possess – the mean value of r_e/h for the early- and late-type spirals from de Jong’s sample of ‘face-on’ galaxies is re-derived. Table 1 gives the probability that the early- and late-type spirals have the same mean r_e/h value depends only mildly on the passband used; the bluer passbands yielding the greatest distinction between the mean r_e/h value for the early- and late-types. Although, in general, the mean r_e/h value is larger for the early-type spirals than the late-type spirals, the difference is not particularly significant. The increased probability in Student’s t-test when certain galaxies are excluded is, to a degree, because of the reduced number of galaxies and consequent lack of strength in the statistical test. Although, the presence of a bar does appear to bias the mean r_e/h value for the early-type spirals. de Jong (1996a) found that he obtained a better fit for 23 of the 86 spiral galaxies when he included an additional bar component in the 2D analysis. After the removal of those 23 barred galaxies, the mean r_e/h values are in agreement with each other.

The robustness of this result is investigated against further modifications to the actual sample used. Inclusion of the few S0 and Irregular type galaxies did not change the probabilities by more than a few percent (and by no more than 1% for those probabilities less than 10%). Exclusion of the Scd galaxies from the late-type sample changed the mean r_e/h value by only 0.002–0.006, but the smaller galaxy numbers in the sample meant that the strength of Student’s t-test was reduced and the probabilities increased because of this.

4.2. Bulge-to-disk luminosity ratio

The bulge-to-disk luminosity ratio is commonly thought to be a fundamental characteristic to the Hubble sequence, and by this it is meant the revised Hubble sequence of Sandage (1961), such

that the prominence of the bulge decreases with the later spiral galaxy types. Sandage had however changed the defining criteria to that of the spiral arms, and so to investigate the above belief, the present galaxy sample was again separated into early- and late-types and Student's t-test employed to measure the probability that the two $\log(B/D)$ luminosity ratio distributions have different mean values. Table 2 shows that the probability that the mean $\log(B/D)$ luminosity ratios could be as different as they are just by chance is less than 0.3% (3σ). The F-test reveals that the two $\log(B/D)$ ratio distributions have similar variances, and so only the results from Student's t-test with similar variances is shown.

While the r_e/h ratio, and similarly $(r_e/h)^2$, are not responsible for the significantly different mean $\log(B/D)$ ratios from the early- and late-type spiral galaxy sets, the other two components to equation 4 are. That is, both the mean difference in the surface brightness term $\log(I_e/I_0)$ and the structural differences given by n are different for the two samples, and responsible for the B/D luminosity ratio decreasing with increasing T -type. The logarithm of the B/D luminosity ratio has been plotted as a function of galaxy type in Figure 14. Within each T -type, while the spread of values can be large, the mean value steadily decreases from type $T=1$ (Sa) to $T=8$ (Sdm). Although, from the $\log(B/D)$ ratio alone it is not possible to state with confidence the morphological type; a conclusion also reached by Simien & de Vaucouleurs (1986) and evident in Figure 1. Perhaps this isn't surprising given that the first criteria of galaxy classification refers to the nature (pitch angle and resolution) of the spiral arms – which must have a somewhat similarly loose correlation with the $\log(B/D)$ ratio. The greater degree of scatter in the K -band is likely to be tied in with how the pitch-angle and spiral-arm nature change once the obscuring dust 'mask' is penetrated at near-infrared wavelengths (Block & Puerari 1999), and the optical Hubble classifications are no longer entirely appropriate.

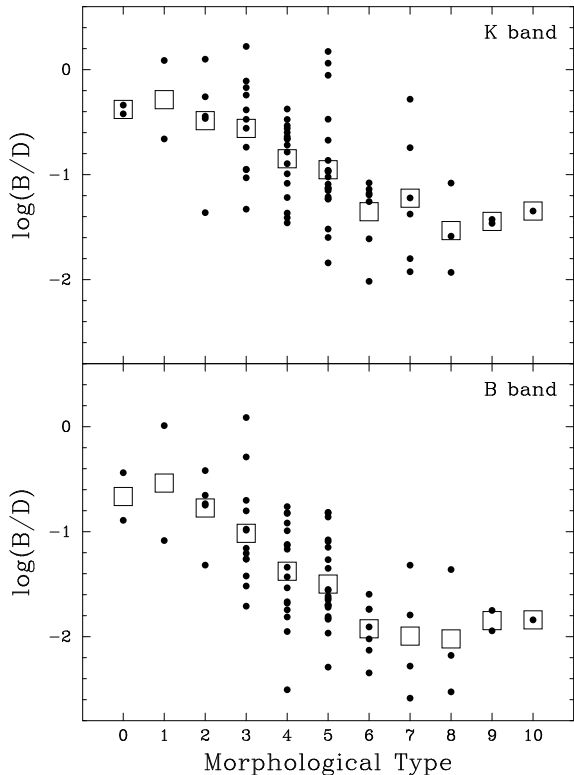


Fig. 14.— The logarithm of the Sérsic bulge to exponential disk luminosity, as given in equation 4, is plotted against morphological type. The disk luminosity has been corrected for inclination effects as described in the text. The squares mark the mean value for each galaxy type.

5. Other quantitative galaxy classification parameters of bulge strength

5.1. The concentration index

Morgan & Mayall (1957) found the spectroscopic characteristics (stellar populations) from the inner parts of a galaxy correlated well with the central concentration of luminosity. Noting the lack of agreement between the spiral arm structure and the nuclear region for many galaxies, Morgan (1958, 1959, 1962) excluded the former criteria from his qualitative classification scheme which was based on the central concentration of light (known as the Yerkes system). de Vaucouleurs (1977) made this method of classification quantitative with the introduction of the concentration index C_{31} , defined as the ratio between the radii that contain 75% and 25% of the total luminosity. Okamura, Kodaira, & Watanabe (1984) showed that the different concentration indices one could construct are essentially the same, and so variations came into use. For example, Kent (1985) used the 20% and 80% radii, while Gavazzi, Gavazzi, & Boselli (1990) replaced the total magnitude with the V magnitude enclosed by the 25 mag arcsec^{-2} isophote.

Doi et al (1992) and Doi, Fukugita, & Okamura (1993) suggested the use of the concentration index for the automatic classification of nearby, and small and faint, galaxies rather than as a means to characterise morphological type. Since then, a small industry has been established (Abraham et al. 1994; Fukugita et al. 1995) and the concentration index has become a popular diagnostic for high redshift galaxies, where the nature of the spiral arms is less clear. Its use has continued for studies of nearby galaxies, most recently in the near-infrared, where Moriondo et al. (1999) used C_{31} at $H_{21.5}$, and Gavazzi et al. (2000) used C_{31} at H_T . In this paper the K -band value for C_{31} is derived within the $K_{22.0}$ mag arcsec^{-2} isophote, and the B -band value for C_{31} is derived using the $B_{25.0}$ mag arcsec^{-2} isophote. The value for C_{31} was also derived using the total galaxy light, but this had little difference on the overall trends and so is not presented here.

Figure 15 reveals, not surprisingly, a somewhat similar behaviour to that seen in Figure 14, but with perhaps slightly less scatter. It would appear that one cannot use the concentration index,

or the B/D ratio, to determine a galaxy's morphological type – an issue taken to heart by Abraham (1999), where it is suggested, at least for studies of distant galaxies, that morphological type be replaced by more quantitative measures. A similar behaviour to that seen in Figure 15 is evident in the H -band data set of Moriondo et al. (1999), where the later type spiral galaxies, from a sample of nearby galaxies, all tend to have low concentration indices around 0.4 – as expected for bulgeless disks – and several of the early-type spiral galaxies also have low concentration indice values.

The logarithm of the concentration index has been plotted against the logarithm of the B/D luminosity ratio in Figure 16. The scatter in the relationship along the lower right of the curve is because C_{31} has been computed using the total galaxy magnitude within some limiting isophote, rather than extrapolating to infinity as was done with the B/D ratio. The increased scatter for B/D ratios greater than about ~ 0.3 arises because sometimes the bulge light is no longer concentrated within the radius containing 25% of the total galaxy light. Consequently, the concentration index is not a good tracer of the logarithm of the B/D luminosity ratio when the bulge is relatively large and extended in comparison to the disk. Use of the 40% and 80% radii improved things a little at the high B/D ratio end of this relation, but at the expense of sensitivity at the low B/D ratio end – that is, most galaxies with B/D ratios less than 0.1 ended up having roughly the same concentration index.

5.2. Two new parameters to measure the apparent prominence of the bulge

Certainly not rejecting the concentration index at this point, this section does however explore other quantitative estimators of bulge strength. While the r_e/h ratio may be useful for galaxy modellers, it apparently does not correlate strongly with the assigned morphological type of a galaxy, nor does it necessarily reflect the 'apparent' prominence of the bulge. Due to the over-lapping of the bulge and disk, what the eye sees (which is what has been used to classify galaxy type) can be misleading and has given rise to this apparent contradiction. Therefore, two new quantitative estimators of bulge strength which more accurately reflect what the eye discerns when it looks an an im-

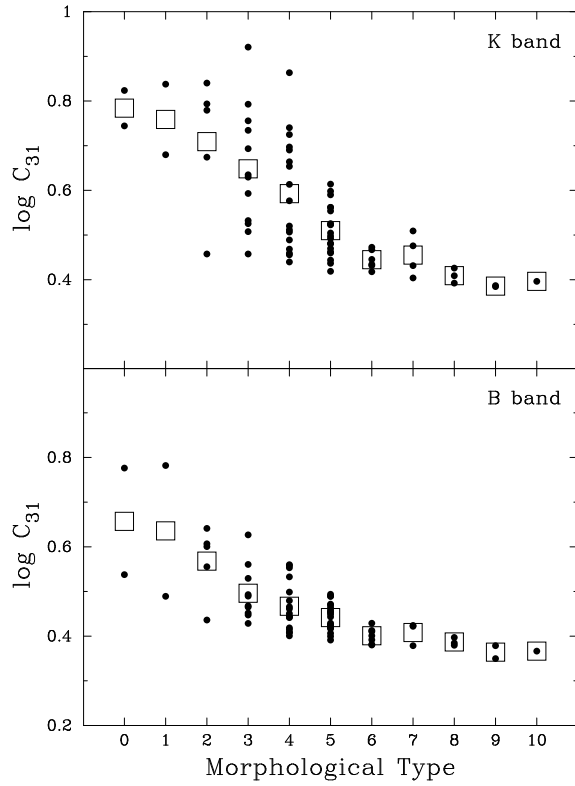


Fig. 15.— The logarithm of the concentration index C_{31} , as defined in the text, is plotted against morphological type.

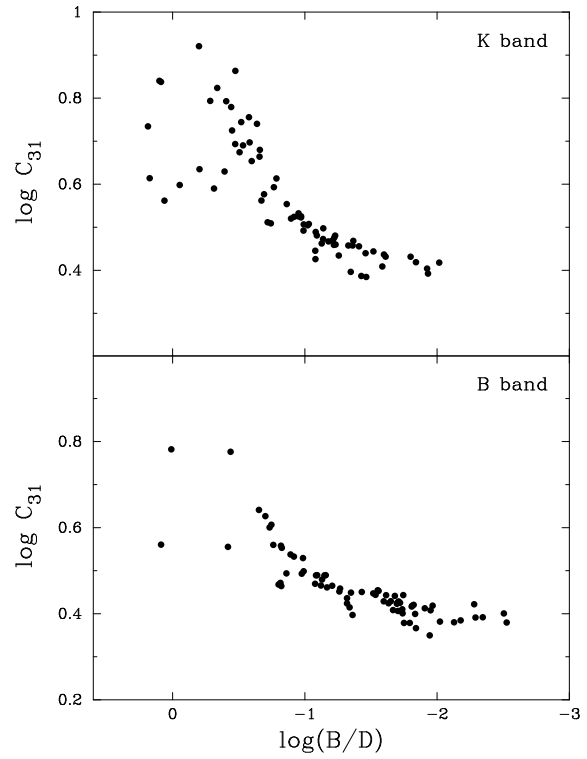


Fig. 16.— The logarithm of the concentration index C_{31} , as defined in the text, is plotted against the logarithm of the bulge-to-disk luminosity ratio.

age of a spiral galaxy are introduced. This should allow us to test if the galaxy sample is perhaps unusual and not representative of the larger galaxy population.

Firstly, the difference between the observed central surface brightness of the galaxy and the surface brightness where the bulge and the disk contribute equally was used as a quantitative measure for the prominence of the bulge. Although the observed central surface brightness will be affected by seeing, because morphological classification is also done with seeing affected images this is the value that has been chosen. There was another motive for using this value rather than the seeing-corrected value, even though this latter quantity is the more appropriate one to use. The reason was to make the result independent of any fitted light profile model.

The situation is a little more complicated with the K -band data. Due to the transparent nature of the disk, the apparent radius where the bulge and disk light contribute equally will actually be dependent on the inclination of the disk, and so the disk surface brightness should first be corrected to some standard value – corrections to the face-on value were applied. Due to this effect, in the K -band, one would expect the observed prominence of the bulge to be less for a sample of highly inclined galaxies than a sample of low-inclination galaxies. Additionally, this will make near-infrared classifications which are based on the prominence of the bulge prone to error.

The average difference between the central galaxy surface brightness and the surface brightness where the bulge and disk light contributes equally was computed for both the early-type ($T \leq 3$) and late-type ($T \geq 6$) spiral galaxies, and the individual data for all galaxies is shown in Figure 17. Application of Student's t-test (Table 3) revealed the probability that the early- and late-type samples could have the same mean difference can be ruled out at greater than the 2σ significance level. This is not a result of the Sérsic models with large n having steeply rising light profiles at their centers; this result is completely independent of the profile models. If we had of used the seeing-corrected, model dependent, central surface brightness values, then this result would be even stronger. That the early-type spiral galaxies have, on average, a greater

difference between the central surface brightness and the surface brightness where the bulge and disk are equally bright, is in accord with expectations, and so it seems probable that the galaxy sample is not peculiar or biased. This gives some reassurance that the r_e/h results presented earlier are likely to be accurate for the population as a whole.

From the plot of $\mu_{\text{central}} - \mu_{\text{bulge=disk}}$ one point stands out in Figure 17. The galaxy UGC 10083, catalogued as (R)SB(r)ab ($T=2$) in NED, does not have an obvious bulge and has a small value for $\mu_{\text{central}} - \mu_{\text{bulge=disk}}$. Inspection of it's image and profile suggest that this galaxy may be more like an Sbc or Sc galaxy (2 or 3 Hubble T types from it's catalogued value; which is perhaps not unreasonable, Lahav et al. 1995). To use Figure 17 again as a diagnostic tool, it is noted that NED gave UGC 09024 the morphological type 'S?'. It has a value for $\mu_{\text{central}} - \mu_{\text{bulge=disk}}$ of around $5.3 \text{ mag arcsec}^{-2}$ (K -band) and $4.0 \text{ mag arcsec}^{-2}$ (B -band), suggesting it's type index is probably around $T=3 \pm 2$.

The second test uses the radius where the surface brightness of the disk and the bulge are equal; that is, the radius where the bulge starts to contribute less light than the disk. To allow for different galaxy sizes, this radius was divided by the radius where the surface brightness of the galaxy is equal to 22 K -mag for the K -band data, and 25 B -mag for the B -band data. It was also separately normalised by dividing by the scale-length of the disk. The results are presented in Figure 18 and Figure 19, and Table 4.

The early-type galaxy sample used here does indeed 'appear' to have, on average, larger bulges than the late-type sample. So how does one interpret the r_e/h data which suggests that the relative size of the bulge and disk is independent of morphological type? The simple answer comes from a terrestrial analog – icebergs. If the bulge is somewhat submerged within the disk, achieved by turning down the bulge stellar density relative to the disk, then only the central peak of the bulge will be visible above the flux of the disk light. Increasing the bulge stellar density will rise the bulge up out of the disk, while the relative scale-length ratio remains unchanged. This iceberg-like scenario is illustrated in Figure 20. Of course, the difference between bulges of early- and late-type spiral

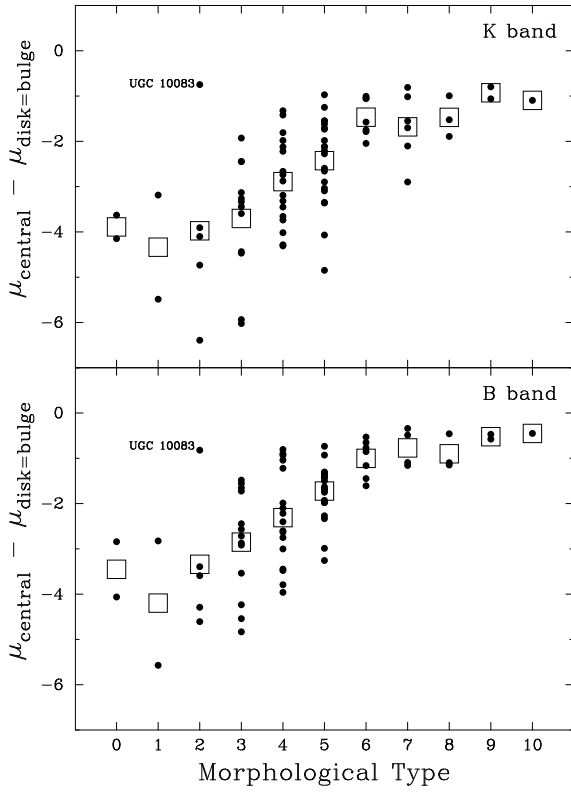


Fig. 17.— The difference between the central galaxy surface brightness and the surface brightness where the bulge and disk light contribute equally is plotted against galaxy morphological type. The effects of seeing are deliberately not taken into account.

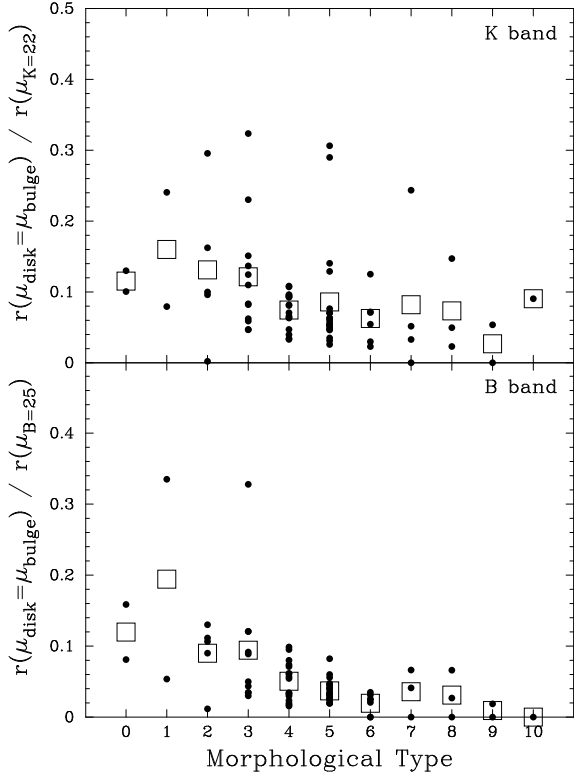


Fig. 18.— The radius where the bulge and disk light contribute equally, normalised by the indicated isophotal radius, is plotted against galaxy morphological type.

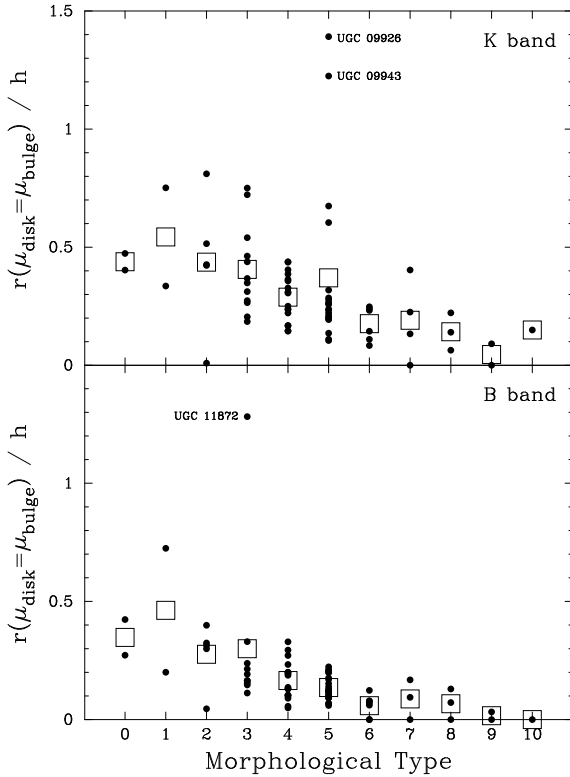


Fig. 19.— The radius where the bulge and disk light contribute equally, divided by the disk scale-length h , is plotted against galaxy morphological type.

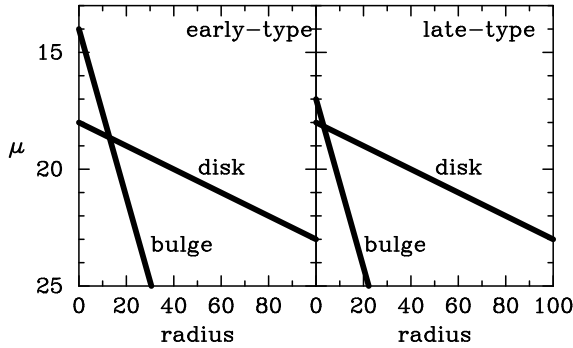


Fig. 20.— This simple schematic illustrates how differences in the relative stellar density between the bulge and disk can produce the optical illusion that galaxies have different bulge-to-disk size ratios. For the exponential models used here, the slope is proportional to the scale-length; the bulge-to-disk scale-length ratio is identical in both panels.

galaxies is more than a case of adjusting the relative bulge/disk intensity, as the profile shapes also vary along the spiral Hubble sequence. However, as a rule, the relative bulge/disk intensity appears to be a characteristic of the Hubble sequence of spiral galaxies.

6. Conclusions

The shape parameters of the spiral galaxy bulges in this sample vary from $n \sim 0.5$ to 4. The results of previous studies which found such variation not to be random but to be systematic with Hubble type, such that late-type spiral galaxies have smaller shape parameters than early-type spiral galaxies, are confirmed. Uncertainties on the model parameters, due to the uncertainty in the sky-background level, are small enough to exclude the possibility that all bulge profile shapes may be the same (i.e. for example $n=4$) and justify the need for using an $r^{1/n}$ bulge model. Moreover, the $r^{1/n}$ bulge models result in a significantly better fit to the bulge than either the classical $r^{1/4}$ or exponential bulge model. This brings attention to the issue of simply using an $r^{1/4}$ law and exponential disk model for disk ellipticals, whose bulge is also likely to be described by an $r^{1/n}$ profile. Not only, in some cases not all, may the disk from such fits be an artifact, or left-over, from an inappropriately fitted $r^{1/4}$ law, but the bulge and disk model parameters will be in error to some degree from the forcing of a classical fitting function to the bulge.

Fitting exponential light profile models to the bulges of spiral galaxies respectively under- and over-estimates the bulge sizes of early- and late-type spiral galaxies; to the degree that one obtains a smaller mean r_e/h ratio for the former rather than the latter (Graham & Prieto 1999a). Fitting an $r^{1/n}$ bulge model reverse this result; however, not to the degree that the mean r_e/h ratios are significantly different between the early- and late-type samples. In contrast, the B/D luminosity ratios are significantly ($>3\sigma$) larger for the early-type spiral galaxies than the late-type spiral galaxies.

It is the relative bulge-to-disk stellar density ratio, not size ratio, that results in the apparent prominence of the bulge and trend with Hubble type. Although, for a given disk size, the disk

surface brightness in late-type spiral galaxies is fainter than in early-type spiral galaxies (Graham 2000), the surface brightness of the bulge in late-type spiral galaxies is yet fainter still, while the bulge-to-disk size ratio is the same. One then has the picture for bulges in late-type galaxies as submerged beneath the surface brightness level of the disk – somewhat akin to an iceberg scenario.

A strong correlation exists between the shape of the bulge light profile and the B/D luminosity ratio. Spiral galaxy bulges do not all have exponential light distributions, less than 10% do. Similarly, the correlation between the shape of the bulge light profile and the bulge luminosity, in both the B - and K -bands, suggests that it may be the mass of the bulge which dictates the stellar distribution in the bulge.

That the Fundamental Plane (Djorgovski & Davis 1987; Dressler et al. 1987) of elliptical galaxies and spiral galaxy bulges (Bender, Burstein, & Faber 1992) are similar, despite their fundamental structural differences (Figure 13), is intriguing. The formation mechanisms at work in the Universe must be such that their structural differences are compensated by dynamical differences in order to give rise to the physical scaling laws that define the Fundamental Plane. This is very likely a reflection of the virial theorem (Faber et al. 1987), with the observed ‘tilt’ explained by a combination of rotational support, non-homology in the velocity dispersion, and stellar population differences (Gregg 1992; Guzmán & Lucey 1993; Bender, Saglia, & Gerhard 1994; Prugniel & Simien 1994, 1997; D’Onofrio, Longo, & Capaccioli 1995; Pahre, Djorgovski, & de Carvalho 1995; Ciotti, Lanzoni, & Renzini 1996; Busarello et al. 1997; Graham & Colless 1997; and a wealth of others). Why then, the dwarf elliptical galaxies, rather than the bulges of spiral galaxies, depart from the Fundamental Plane of ordinary elliptical galaxies adds to the intrigue, and may be explained when the above second order effects are fully dealt with for all classes of objects. Another question relating to the measured magnitude is the issue of extrapolation of the light profiles to infinity or the truncation at some isophotal radius possibly limited by the sky background light.

I wish to thank Mercedes Prieto for initiating this study, and Nicola Caon and Helmut Jerjen

for providing me with the ‘ordinary’ and dwarf elliptical galaxy data which was used to construct Figure 13. This research has made use of the NASA/IPAC Extragalactic Database (NED) which is operated by the Jet Propulsion Laboratory, California Institute of Technology, under contract with the National Aeronautics and Space Administration.

REFERENCES

Abraham, R.G. 1999, in *Toward a New Millennium in Galaxy Morphology*, Ap&SS, 269, 323

Abraham, R.G., Valdes, F., Yee, H.K.C., & van den Bergh, S. 1994, ApJ, 432, 75

Andredakis, Y.C., Peletier, R.F., & Balcells, M. 1995, MNRAS, 275, 874

Bender, R., Saglia, R.P., & Gerhard, O.E. 1994, MNRAS, 269, 785

Bender, R., Burstein, D., & Faber, S.M. 1992, ApJ, 399, 462

Binggeli, B., & Cameron, L.M. 1991, A&A, 252, 27

Binggeli, B., & Cameron, L.M. 1993, A&AS, 98, 297

Binney, J., & Merrifield, M. 1998, *Galactic Astronomy*, Princeton University Press, Princeton, New Jersey, p.220

Block, D.L., & Puerari, I. 1999, A&A, 342, 627

Burstein, D., & Heiles, C. 1984, ApJS, 54, 33

Busarello, G., Capaccioli, M., Capozziello, S., Longo, G., & Puddu, E. 1997, A&A, 320, 415

Caldwell, N., & Bothun, G.D. 1987, AJ, 94, 1126

Caon, N., Capaccioli, M., & D’Onofrio, M. 1993, MNRAS, 265, 1013

Capaccioli, M. 1987, in *Structure and Dynamics of Elliptical Galaxies*, IAU Symp. 127, Reidel, Dordrecht, p.47

Capaccioli, M. 1989, in *Le Monde des Galaxies*, Springer-Verlag, Berlin, p.208

Ciotti, L., Lanzoni, B., & Renzini, A. 1996, MNRAS, 282, 1

Courteau, S., de Jong, R.S., & Broeils, A.H. 1996, ApJ, 457, L73

Davies, J.I., Phillipps, S., Cawson, M.G.M., Disney, M.J., & Kibblewhite, E.J. 1988, MNRAS, 232, 239

de Jong, R.S. 1996a, A&AS, 118, 557

de Jong, R.S. 1996b, A&A, 313, 45

de Jong, R.S., & van der Kruit, P.C. 1994, A&AS, 106, 451

de Vaucouleurs, G. 1948, Ann. d'Astrophys., 11, 247

de Vaucouleurs, G. 1959, Hdb. d. Physik, 53, 311

de Vaucouleurs, G. 1977, in Evolution of Galaxies and Stellar populations, eds. R. Larson & B. Tinsley (New Haven: Yale University Observatory) p.43

de Vaucouleurs, G., de Vaucouleurs, A., Corwin, H.G., Buta, R.J., Paturel, G., & Fouque, P. 1991, Third Reference Catalog of Bright Galaxies (Springer-Verlag, New York)(RC3)

Djorgovski, S., & Davis, M. 1987, ApJ, 313, 59

Doi, M., Kashikawa, N., Okamura S., Tarusawa. K., Fukugita, M., Sekiguchi, M., & Iwashita, H. 1992, in Digitised Optical Sky Surveys, Kluwer, Dordrecht, p.199

Doi, M., Fukugita, M., & Okamura, S. 1993, MNRAS, 264, 832

D'Onofrio, M., Capaccioli, M., & Caon, N. 1994, MNRAS, 271, 523

D'Onofrio, M., Longo, G., & Capaccioli, M. 1995, in Fresh Views of elliptical galaxies, ASP Conf. Ser., 86, 143

Dressler, A., Lynden-Bell, D., Burstein, D., Davies, R.L., Faber, S.M., Terlevich, R.J., & Wegner, G. 1987, ApJ, 313, 42

Faber, S.M., Dressler, A., Davies, R.L., Burstein, D., Lynden-Bell, D., Terlevich, R.J., & Wegner, G. 1987, in Nearly Normal Galaxies, Springer, New York, p.175

Freeman, K.C. 1970, ApJ, 160, 811

Fukugita, M., Doi, M., Dressler, A., & Gunn, J.E. 1995, ApJ, 439, 584

Gavazzi, G., Franzetti, P., Scodéglio, M., Boselli, A., & Pierini, D. 2000, A&A, in press, (astro-ph/0007411)

Gavazzi, G., Garilli, B., & Boselli, A. 1990, A&AS, 83, 399

Gerbal, D., Lima Neto, G.B., Márquez, I., & Verhagen, H. 1997, MNRAS, 285, L41

Giovanelli, R., Haynes, M.P., Salzer, J.J., Wegner, G., Da Costa, L.N., & Freudling, W. 1994, AJ, 107, 2036

Graham, A.W., Lauer, T., Colless, M.M., & Postman, M. 1996, ApJ, 465, 534

Graham, A.W., & Colless, M.M. 1997, MNRAS, 287, 221

Graham, A.W. 1998, MNRAS, 295, 933

Graham, A.W., & Prieto, M. 1999a, ApJ, 524, L23

Graham, A.W., & Prieto, M. 1999b, in Toward a New Millennium in Galaxy Morphology, Ap&SS, 269, 653

Graham, A.W. 2000, MNRAS, submitted

Graham, A.W., & Prieto, M. 2000a, in Galaxy Disks and Disk Galaxies, PASP, in press

Graham, A.W., & Prieto, M. 2000b, in The Evolution of Galaxies. I - Observational Clues, Ap&SS, in press

Gregg, M.D. 1992, ApJ, 384, 43

Guzmán, R., & Lucey, J.R. 1993, MNRAS, 263, L47

Hjorth, J., & Madsen, J. 1995, ApJ, 445, 55

Hubble, E. 1926, ApJ, 64, 321

Hubble, E. 1936, in The Realm of the Nebulae (Yale University Press, New Haven)

Jerjen, H., & Binggeli, B. 1997, in The Nature of Elliptical Galaxies; The Second Stromlo Symposium, ASP Conf. Ser., 116, 239

Jerjen, H., Binggeli, B., & Freeman, K.C. 2000, AJ, 119, 593

Jerjen, H., Freeman, K.C., & Binggeli, B. 2000, in prep.

Kent, S. 1985, ApJS, 59, 115

Khosroshahi, H.G., Wadadekar, Y., & Kembhavi, A. 2000, ApJ, 533, 162

Kormendy, J. 1977, ApJ, 217, 406

Lahav, O., Naim, A., Buta, R.J., Corwin, H.G., de Vaucouleurs, G., et al. 1995, Science, 267, 859

Lima Neto, G.B., Gerbal, D., & Márquez, I. 1999, MNRAS, 309, 481

Michard, R. 1985, A&A, 59, 205

Moffat, A.F.J. 1969, A&A, 3, 455

Morgan, W.W. 1958, PASP, 70, 364

Morgan, W.W. 1959, PASP, 71, 394

Morgan, W.W. 1962, ApJ, 135, 1

Morgan, W.W., & Mayall, N.U. 1957, PASP, 69, 291

Moriondo, G., Giovanardi, C., & Hunt, L.K. 1998, A&AS, 130, 81

Moriondo, G., et al. 1999, A&AS, 137, 101

Okamura, S., Kodaira, K., & Watanabe, M. 1984, ApJ, 280, 7

Pahre, M.A., Djorgovski, S.G., & de Carvalho, R.R. 1995, ApJ, 453, L17

Patterson, F.Sh. 1940, Harvard Bull., 914, 9

Poggianti, B.M. 1997, A&AS, 122, 399

Press, W.H., Flannery, B.P., Teukolsky, S.A., & Vetterling, W.T. 1986, Galactic Astronomy, Cambridge University Press, Cambridge, p.176

Prieto, M., Gottesman, S.T., López-Aguerri, J.A., Varela, A.M., AJ, 114, 1413

Prieto, M., López-Aguerri, J.A., Varela, A.M., Muñon-Tuñón, C., 2000, A&A, accepted

Pritchett, C., & Kline, M.I. 1981, AJ, 86, 1859

Prugniel, P., & Simien, F. 1994, A&A, 281, L1

Prugniel, P., & Simien, F. 1997, A&A, 321, 111

Saglia R.P., et al. 1993, MNRAS, 264, 961

Sandage, A. 1961, The Hubble Atlas of Galaxies (Carnegie Institution of Washington, Washington, D.C.)

Schlegel, D.J., Finkbeiner, D.P., & Davis, M. 1998, ApJ, 500, 525

Schombert, J.M. 1986, ApJ, 60, 603

Schombert, J.M., & Bothun, D. 1987, AJ, 92, 60

Sèrsic, J.-L. 1968, Atlas de Galaxias Australes (Cordoba: Observatorio Astronomico)

Simien, F., & de Vaucouleurs, G. 1986, ApJ, 302, 564

Tully, R.B., & Verheijen, M.A.W. 1997, ApJ, 484, 145

van den Bergh, S. 1997, AJ, 113, 2054

Young, C.K., & Currie, M.J. 1994, MNRAS, 268, L11

Young, C.K., & Currie, M.J. 1995, MNRAS, 273, 1141

A. *K*-band light profile data and models

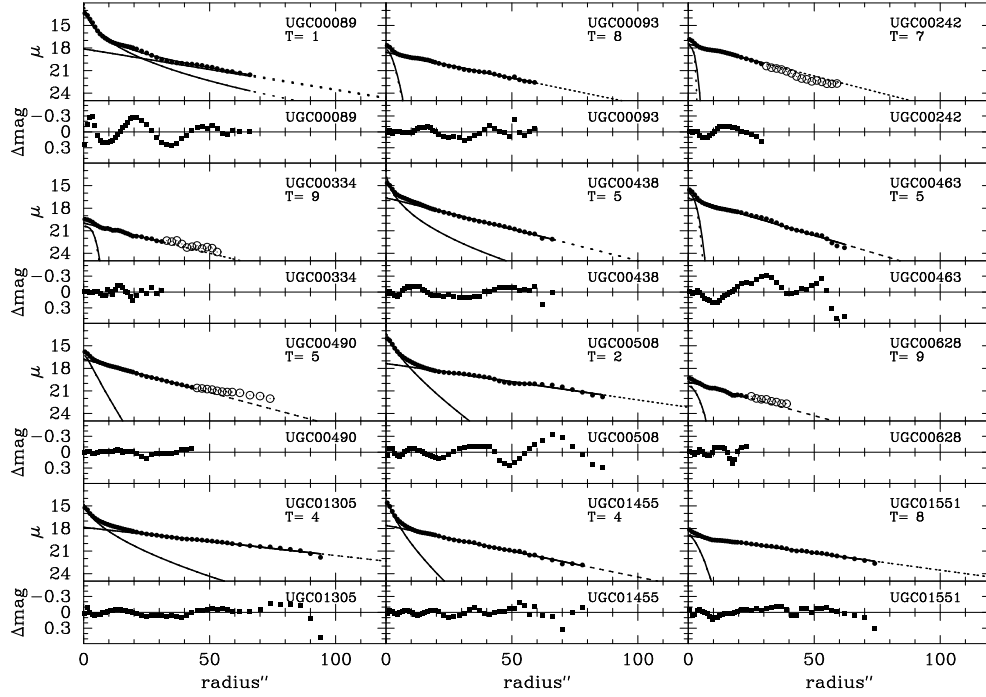


Fig. 21.— The best-fitting seeing convolved $r^{1/n}$ bulge and exponential disk models (solid lines) are fitted to the K -band surface brightness profiles from de Jong (1996a). The dashed lines are the models before they are convolved with the PSF.

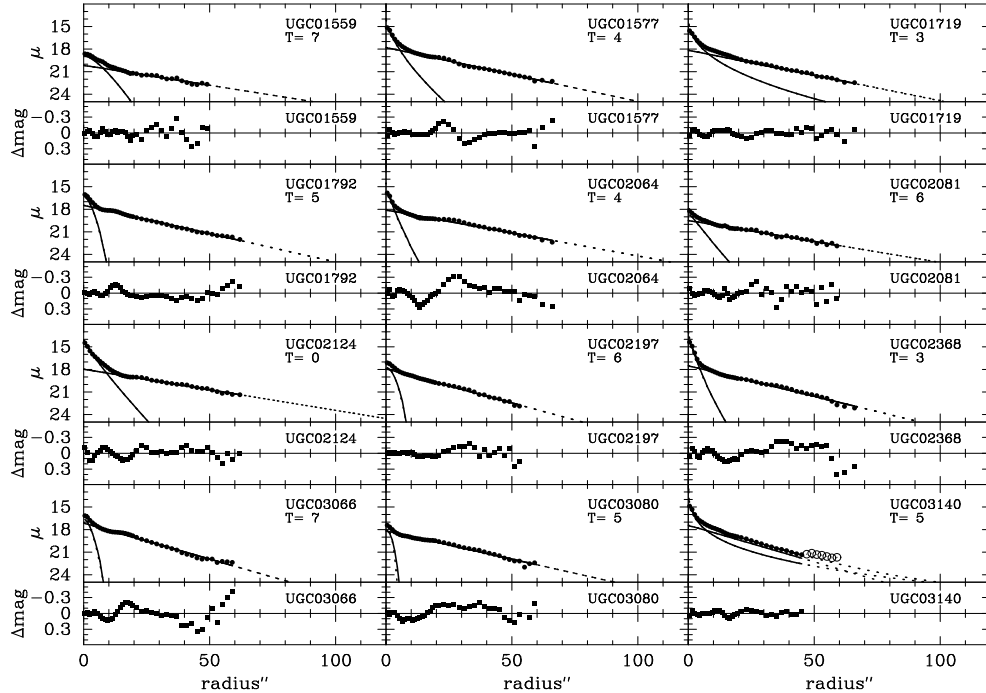


Fig. 22.— *cont.*

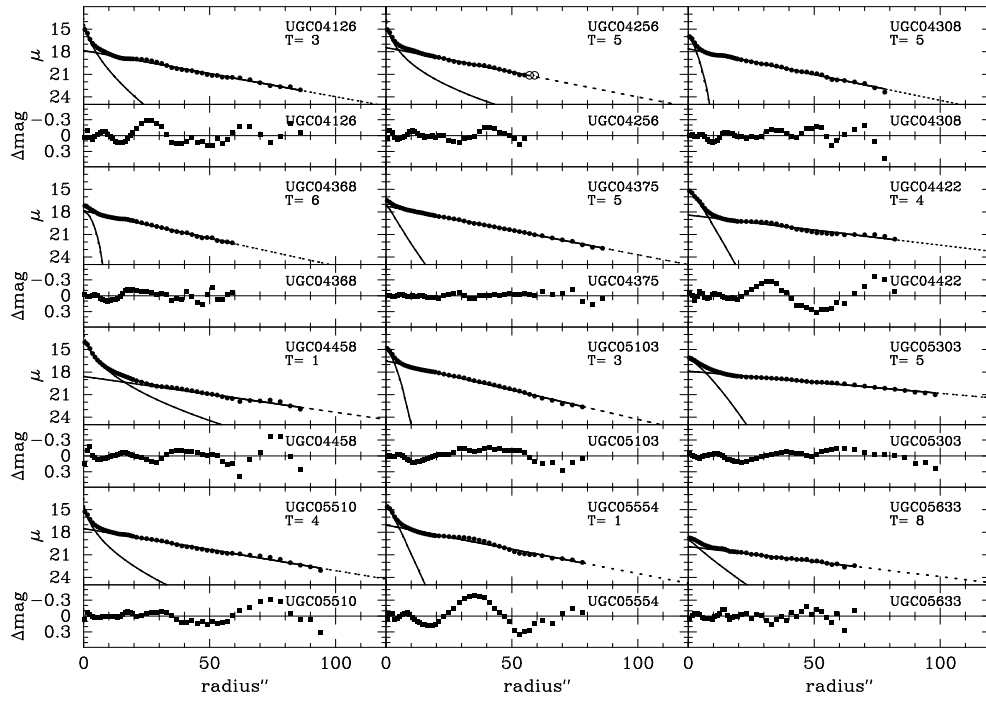


Fig. 23.— *cont.*

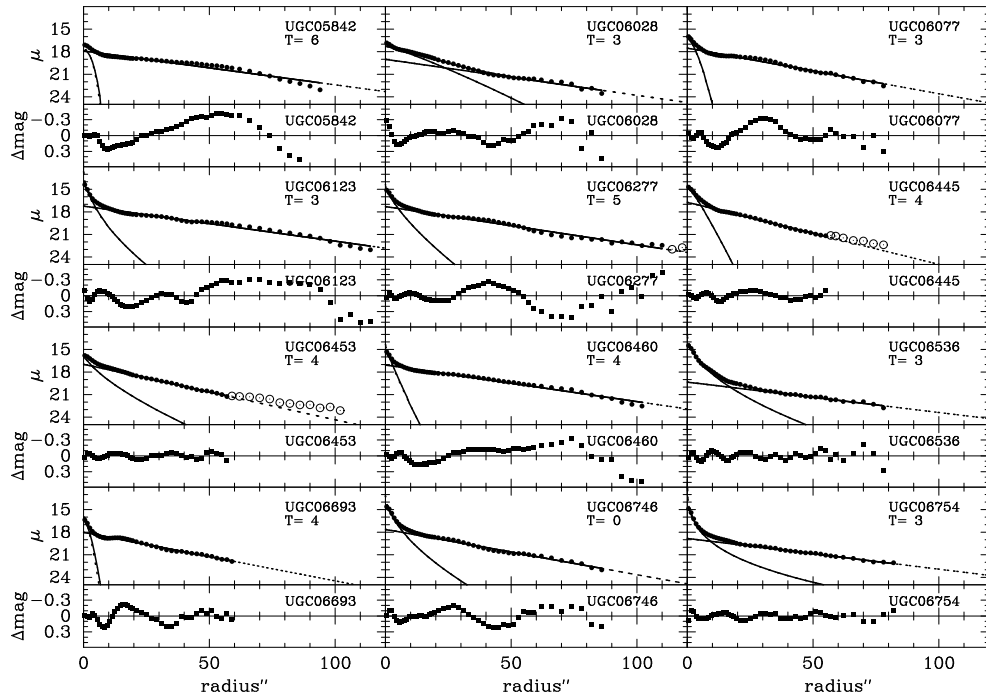


Fig. 24.— *cont.*

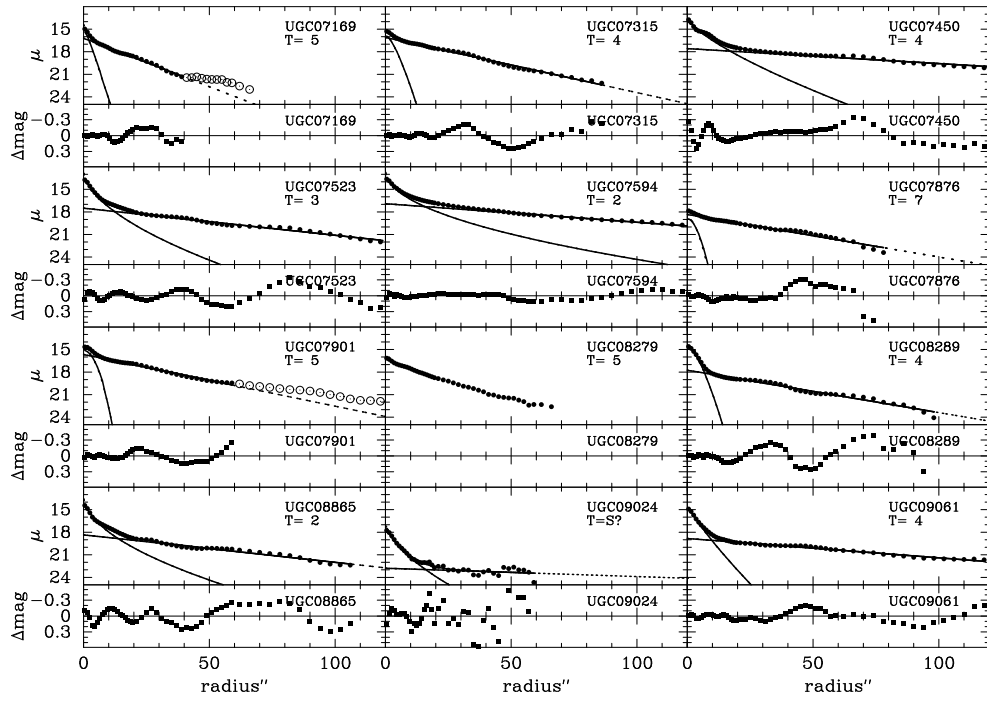


Fig. 25.— *cont.*

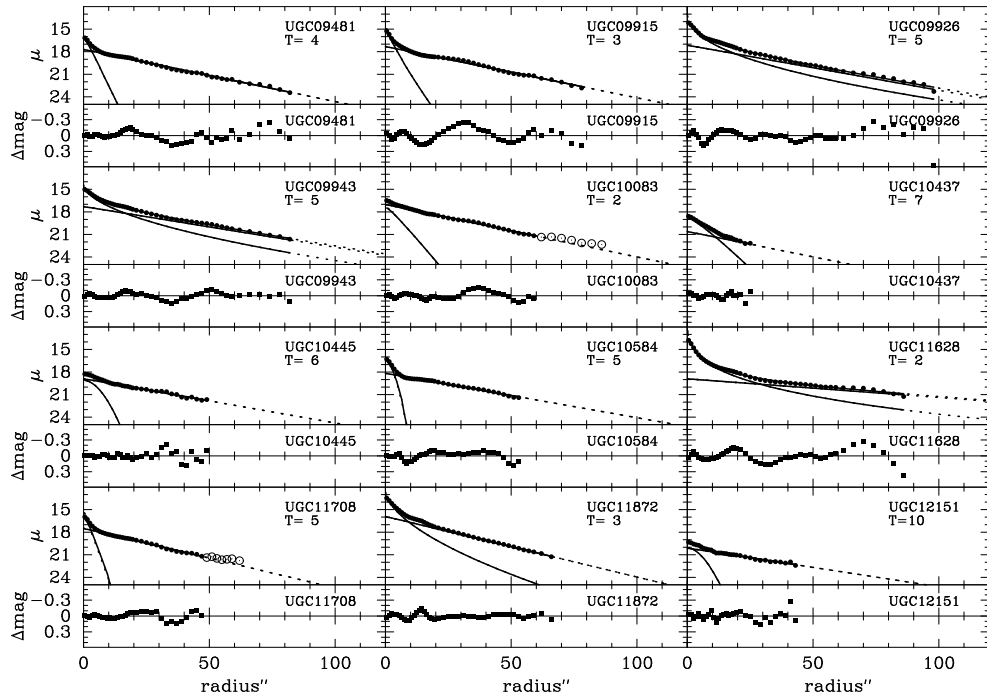


Fig. 26.— *cont.*

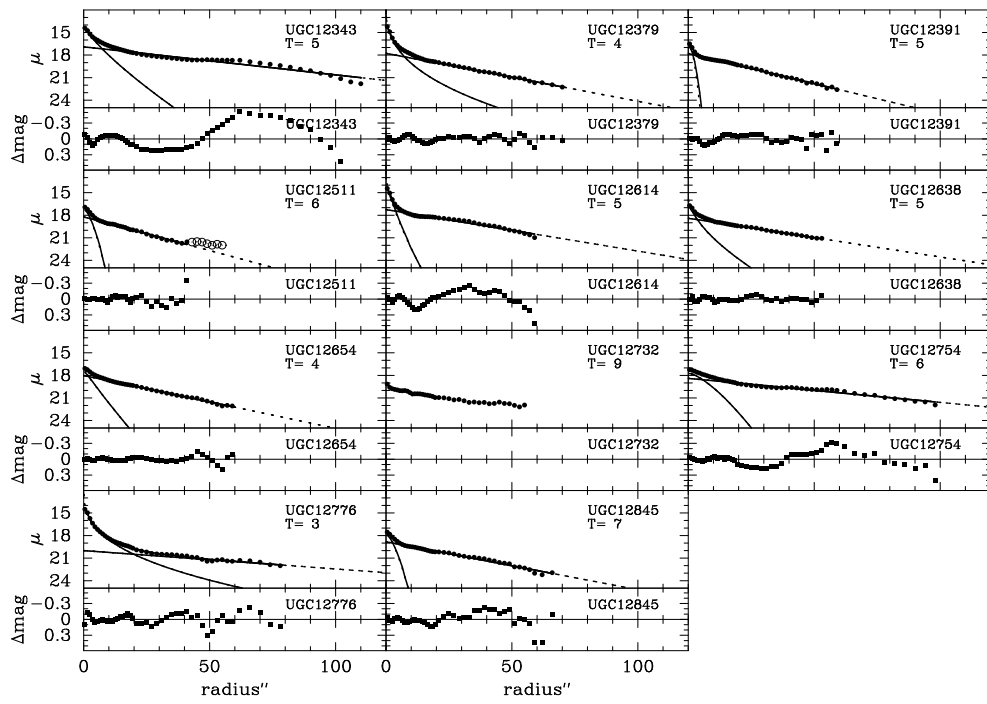


Fig. 27.— *cont.*

TABLE 1
COMPARISON OF THE r_e/h DATA DISTRIBUTIONS

Band	$\langle \frac{r_e}{h} \rangle_{\text{early-type}} - \langle \frac{r_e}{h} \rangle_{\text{late-type}}$	No.	Prob(F)	Prob(t), Prob(t_u)
Total Galaxy Sample				
B	$(0.211 - 0.130) = 0.081$	(20,16)	<.1%	08%, 06%
R	$(0.209 - 0.149) = 0.060$	(20,19)	01%	06%, 06%
I	$(0.241 - 0.183) = 0.058$	(15,18)	01%	13%, 15%
K	$(0.213 - 0.199) = 0.014$	(19,18)	89%	58%, 58%
Excluding galaxies modelled by de Jong to have a bar				
B	$(0.148 - 0.122) = 0.026$	(9,14)	14%	37%, 42%
R	$(0.157 - 0.146) = 0.011$	(9,17)	29%	66%, 62%
I	$(0.250 - 0.183) = 0.067$	(6,17)	01%	18%, 37%
K	$(0.181 - 0.195) = -0.014$	(8,16)	23%	66%, 61%
Excluding galaxies that had their outer profile truncated				
B	$(0.194 - 0.135) = 0.059$	(17,15)	<.1%	19%, 18%
R	$(0.207 - 0.167) = 0.040$	(18,15)	0.5%	27%, 24%
I	$(0.212 - 0.192) = 0.020$	(13,16)	09%	56%, 56%
K	$(0.214 - 0.203) = 0.011$	(18,14)	65%	75%, 74%

NOTE.—Comparison of the r_e/h data distributions for the early-type (Sa,Sab,Sb) and late-type (Scd,Sd,Sdm,Sm) spiral galaxies. Column 1 shows the passband used. The difference between the mean values of r_e/h from the two distributions is shown in column 2, while Column 3 gives the number of galaxies in the early- and late-type samples respectively. Column 4 shows the probability, from an F-test, that the two distributions of r_e/h have different variances (small values indicate significantly different variances – in which case Student's t-test with unequal variances should be used). Column 5 gives the probability that the two distributions have the same mean value, as derived from Student's t-test assuming equal, Prob(t), and unequal, Prob(t_u), variances. Small probabilities indicate that the two data sets have significantly different means.

TABLE 2
COMPARISON OF THE $\log(B/D)$ DATA DISTRIBUTIONS

Band	$\langle \log \frac{B}{D} \rangle_{early-type} - \langle \log \frac{B}{D} \rangle_{late-type}$	No.	Prob(F)	Prob(t)
Total Galaxy Sample				
B	$(-0.91 -- 1.95) = 1.04$	(20,16)	31%	$4.10^{-06} \%$
R	$(-0.72 -- 1.65) = 0.93$	(20,19)	88%	$2.10^{-05} \%$
I	$(-0.62 -- 1.45) = 0.83$	(15,18)	40%	$3.10^{-04} \%$
K	$(-0.54 -- 1.35) = 0.81$	(19,18)	91%	$3.10^{-04} \%$
Excluding galaxies modelled by de Jong to have a bar				
B	$(-1.07 -- 2.02) = 0.95$	(9,14)	19%	$3.10^{-03} \%$
R	$(-0.87 -- 1.67) = 0.80$	(9,17)	97%	$4.10^{-02} \%$
I	$(-0.61 -- 1.46) = 0.85$	(6,17)	20%	$6.10^{-02} \%$
K	$(-0.65 -- 1.38) = 0.73$	(8,16)	62%	$2.10^{-01} \%$
Excluding galaxies that had their outer profile truncated				
B	$(-0.88 -- 1.92) = 1.04$	(17,15)	23%	$3.10^{-05} \%$
R	$(-0.66 -- 1.56) = 0.90$	(18,15)	83%	$2.10^{-04} \%$
I	$(-0.57 -- 1.42) = 0.85$	(13,16)	61%	$4.10^{-04} \%$
K	$(-0.46 -- 1.32) = 0.86$	(18,14)	64%	$8.10^{-04} \%$

NOTE.—Comparison of the $\log(B/D)$ data distributions for the early- and late-type spiral galaxies. Column 1 shows the passband used, while column 2 shows the difference between the mean $\log(B/D)$ values from the early- and late-type distributions. Column 3 gives the number of galaxies in the early- and late-type samples. Column 4 shows the probability that the two distributions have different variances (small values indicate significantly different variances). Column 5 gives the probability that the two distributions have the same mean value – as derived from Student’s t-test. The disk surface brightness has been corrected for inclination according to the prescripts given in the text.

TABLE 3
COMPARISON OF THE $\mu_{cen} - \mu_{b=d}$ DATA DISTRIBUTIONS

Band	$\left\langle \log \frac{I_{cen}}{I_{b=d}} \right\rangle_{early-type} - \left\langle \log \frac{I_{cen}}{I_{b=d}} \right\rangle_{late-type}$	No.	Prob(F)	Prob(t), Prob(t_u)
Total Galaxy Sample				
B	(-3.11 - -0.87) = -2.24	(20,16)	<.1%	$1.10^{-5}\%$, $2.10^{-5}\%$
R	(-3.44 - -1.32) = -2.12	(20,19)	0.2%	$5.10^{-5}\%$, $1.10^{-4}\%$
I	(-3.64 - -1.43) = -2.22	(15,18)	<.1%	$4.10^{-5}\%$, $2.10^{-3}\%$
K	(-3.84 - -1.48) = -2.36	(19,18)	<.1%	$2.10^{-5}\%$, $1.10^{-4}\%$
Excluding galaxies modelled by de Jong to have a bar				
B	(-2.71 - -0.79) = -1.92	(9,14)	<.1%	$9.10^{-3}\%$, $4.10^{-1}\%$
R	(-3.03 - -1.32) = -1.72	(9,17)	01%	$3.10^{-2}\%$, $6.10^{-1}\%$
I	(-3.69 - -1.43) = -2.265	(6,17)	<.1%	$5.10^{-3}\%$, $2.10^{-0}\%$
K	(-3.69 - -1.43) = -2.26	(8,16)	0.1%	$4.10^{-3}\%$, $5.10^{-1}\%$
Excluding galaxies that had their outer profile truncated				
B	(-3.31 - -0.85) = -2.46	(17,15)	<.1%	$4.10^{-6}\%$, $3.10^{-5}\%$
R	(-3.62 - -1.32) = -2.30	(18,15)	02%	$8.10^{-5}\%$, $6.10^{-5}\%$
I	(-3.86 - -1.44) = -2.42	(13,16)	0.1%	$9.10^{-6}\%$, $7.10^{-4}\%$
K	(-4.07 - -1.57) = -2.50	(18,14)	0.4%	$3.10^{-5}\%$, $2.10^{-5}\%$

NOTE.—Comparison of the $(\mu_{cen} - \mu_{b=d})$ data distributions for the early-type (Sa,Sab,Sb) and late-type (Scd,Sd,Sdm,Sm) spiral galaxies. Column 1 shows the passband used. The difference between the mean values of $\log(I_{cen}/I_{b=d})$ from the two distributions is shown in column 2, while Column 3 gives the number of galaxies in the early- and late-type samples. Column 4 shows the probability that the two distributions have different variances (small values indicate significantly different variances – in which case Student's t-test with unequal variances should be used). Column 5 gives the probability that the two distributions have the same mean value, as derived from Student's t-test assuming equal, Prob(t), and unequal, Prob(t_u), variances. Small probabilities indicate that the two data sets have significantly different means. The disk surface brightness has been corrected for inclination according to the prescriptions given in the text.

TABLE 4
COMPARISON OF THE $r_{b=d}/h$ DATA DISTRIBUTIONS

Band	$\langle \frac{r_{b=d}}{h} \rangle_{early-type} - \langle \frac{r_{b=d}}{h} \rangle_{late-type}$	No.	Prob(F)	Prob(t), Prob(t_u)
Total Galaxy Sample				
B	$(0.312 - 0.061) = 0.251$	(20,16)	<.1%	$3.10^{-1}\%$, $3.10^{-1}\%$
R	$(0.360 - 0.126) = 0.234$	(20,19)	<.1%	$1.10^{-2}\%$, $5.10^{-2}\%$
I	$(0.404 - 0.164) = 0.240$	(15,18)	<.1%	$5.10^{-2}\%$, $1.10^{-1}\%$
K	$(0.428 - 0.156) = 0.272$	(19,18)	01%	$9.10^{-3}\%$, $5.10^{-3}\%$
Excluding galaxies modelled by de Jong to have a bar				
B	$(0.268 - 0.050) = 0.218$	(9,14)	<.1%	0.2%, 3%
R	$(0.330 - 0.124) = 0.206$	(9,17)	0.1%	0.2%, 4%
I	$(0.416 - 0.164) = 0.252$	(6,17)	0.2%	0.2%, 5%
K	$(0.399 - 0.151) = 0.248$	(8,16)	01%	0.3%, 2%
Excluding galaxies that had their outer profile truncated				
B	$(0.349 - 0.061) = 0.288$	(17,15)	<.1%	$2.10^{-1}\%$, $4.10^{-1}\%$
R	$(0.389 - 0.137) = 0.252$	(18,15)	<.1%	$3.10^{-2}\%$, $4.10^{-2}\%$
I	$(0.430 - 0.170) = 0.260$	(13,16)	0.1%	$5.10^{-2}\%$, $2.10^{-1}\%$
K	$(0.463 - 0.170) = 0.293$	(18,14)	05%	$2.10^{-2}\%$, $4.10^{-3}\%$

NOTE.—Comparison of the $r_{b=d}/h$ data distributions for the early-type (Sa,Sab,Sb) and late-type (Scd,Sd,Sdm,Sm) spiral galaxies. Column 1 shows the passband used. The difference between the mean values of $r_{b=d}/h$ from the two distributions is shown in column 2, while Column 3 gives the number of galaxies in the early- and late-type samples. Column 4 shows the probability that the two distributions have different variances (small values indicate significantly different variances – in which case Student's t-test with unequal variances should be used). Column 5 gives the probability that the two distributions have the same mean value, as derived from Student's t-test assuming equal, Prob(t), and unequal, Prob(t_u), variances. Small probabilities indicate that the two data sets have significantly different means. The disk surface brightness has been corrected for inclination according to the prescripts given in the text.